



Prospective computational design and *in vitro* bio-analytical tests of new chemical entities as potential selective CYP17A1 lyase inhibitors

N.J. Gumede^{a,*}, W. Nxumalo^b, K. Bisetty^c, L. Escuder Gilabert^d, M.J. Medina-Hernandez^d, S. Sagrado^{d,e}

^a Department of Chemistry, Mangosuthu University of Technology, PO Box 12363, Jacobs 4026, South Africa

^b Department of Chemistry, University of Limpopo, Private Bag X 1106, Sovenga 0727, South Africa

^c Department of Chemistry, Durban University of Technology, PO Box 1334, Durban 4000, South Africa

^d Departamento de Química Analítica, Facultad de Farmacia, Universidad de Valencia, Avda. Vicent Andrés Estellés, s/n, E-46100 Burjassot, Valencia, Spain

^e Instituto Interuniversitario de Investigación de Reconocimiento Molecular y Desarrollo Tecnológico (IDM), Universitat Politècnica de València, Universitat de València, Avda. Vicent Andrés Estellés, s/n, E-46100 Burjassot, Valencia, Spain

ARTICLE INFO

Keywords:

Metastatic-castration resistant prostate cancer
3D-QSAR pharmacophore model
CYP17A1 inhibitors
17,20-lyase selective inhibition
Prospective computational design

ABSTRACT

The development and advancement of prostate cancer (PCa) into stage 4, where it metastasize, is a major problem mostly in elder males. The growth of PCa cells is stirred up by androgens and androgen receptor (AR). Therefore, therapeutic strategies such as blocking androgens synthesis and inhibiting AR binding have been explored in recent years. However, recently approved drugs (or in clinical phase) failed in improving the expected survival rates for this metastatic-castration resistant prostate cancer (mCRPC) patients. The selective CYP17A1 inhibition of 17,20-lyase route has emerged as a novel strategy. Such inhibition blocks the production of androgens everywhere they are found in the body. In this work, a three dimensional-quantitative structure activity relationship (3D-QSAR) pharmacophore model is developed on a diverse set of non-steroidal inhibitors of CYP17A1 enzyme. Highly active compounds are selected to define a six-point pharmacophore hypothesis with a unique geometrical arrangement fitting the following description: two hydrogen bond acceptors (A), two hydrogen bond donors (D) and two aromatic rings (R). The QSAR model showed adequate predictive statistics. The 3D-QSAR model is further used for database virtual screening of potential inhibitory hit structures. Density functional theory (DFT) optimization provides the electronic properties explaining the reactivity of the hits. Docking simulations discovers hydrogen bonding and hydrophobic interactions as responsible for the binding affinities of hits to the CYP17A1 Protein Data Bank structure. 13 hits from the database search (including five derivatives) are then synthesized in the laboratory as different scaffolds. Ultra high performance liquid chromatography-tandem mass spectrometry (UHPLC-MS/MS) *in vitro* experiments reveals three new chemical entities (NCEs) with half maximal inhibitory concentration (IC_{50}) values against the lyase route at mid-micromolar range with favorable selectivity to the lyase over the hydroxylase route (one of them with null hydroxylase inhibition). Thus, prospective computational design has enabled the design of potential lead lyase-selective inhibitors for further studies.

1. Introduction

Prostate cancer (PCa) has emerged as a real danger in elderly male because it is able to develop, grow, relapse and then metastasize [1–7]. The androgens are very important in the biological processes of normal

and diseased prostates [1,8]. First in line therapy to treat PCa includes the use of antiandrogens (i.e. the chemotherapeutic agent docetaxel) as well as the analogues of gonadotropin releasing hormone in combination with androgen receptor (AR) antagonists [9–11]. All these treatment options proved futile in the blockage of androgen biosynthesis in

Abbreviations: NCE, New Chemical Entity; UHPLC, Ultra-High Performance Liquid Chromatography; APCI, Atmospheric Pressure Chemical Ionization; Abiraterone Acetate, AA; Abiraterone, ABT; MRM, Multiple Reaction Monitoring; 3D-QSAR, 3 Dimensional Quantitative Structure Activity Relationship; IFD, Induced Fit Docking; CPH, Common Pharmacophore Hypothesis; DFT, Density Functional Theory; PLS, Partial Least Squares; mCRPC, Metastatic castration resistant prostate cancer

* Corresponding author.

E-mail address: ngumede@mut.ac.za (N.J. Gumede).

<https://doi.org/10.1016/j.bioorg.2019.103462>

Received 3 June 2019; Received in revised form 27 September 2019; Accepted 20 November 2019

Available online 02 December 2019

0045-2068/© 2019 Elsevier Inc. All rights reserved.

all its sources such as the testes and adrenals [12]. The progression of metastatic-castration resistant prostate cancer (mCRPC) is lethal and aggressive; so, there is a great demand to find alternative treatment options in pursuit to increase the overall survival rates of patients suffering from mCRPC [13].

The use of CYP17A1 enzyme as a drug target is an attractive option [14–18]. Its inhibition decreases the levels of circulating androgens, which is thought to be more effective than conventional therapies [1,10,14–20]. The CYP17A1 enzyme is responsible for the catalysis and conversion of progesterone and pregnenolone into 17 α -products, such as 17 α -hydroxyprogesterone and 17 α -hydroxypregnenolone, respectively [4,21,22]. The hydroxylase route is important in cortisol formation. Thus, the inhibition of the formation of cortisol results in mineralocorticoid excess syndrome (MES), which is associated with cardiovascular diseases [20,23]. Accordingly, Bird et al [24] has pointed out that in humans CYP17A1's role is also to catalyze the conversion of 17 α -hydroxypregnenolone to form dehydroepiandrosterone (DHEA) through the lyase route. Therefore, since the lyase route does not undergo MES [20,23], the design of CYP17A1 inhibitors with favorable lyase selectivity over hydroxylase is a promising therapeutic strategy [9,25].

Ketoconazole (KTZ) is an antifungal agent currently used as an off-label drug for PCa therapy targeting the CYP17A1 enzyme [26]. However, its therapeutic effect is outweighed by its toxicity effect [9,27]. Abiraterone (ABT) was discovered and designed to improve the overall survival rates of patients suffering from mCRPC [26]. Abiraterone acetate (AA) attained its approval in 2011 by the US Food and Drug Administration [9,22,26]. The main drawback regarding AA is the dual inhibition of both the 17 α -hydroxylase and the 17,20-lyase routes of CYP17A1 enzyme [23]. Hence, patients on the AA therapy are also given prednisone in order to account for MES [9,13,19,28].

The non-steroidal inhibitors such as orteronel (TAK-700) [28], galeterone (TOK001) [26,27,29,30] and seviteronel (VT-464) [23,31] selectively inhibit the lyase route over the hydroxylase of CYP17A1 enzyme; according to pre-clinical data [9,26]. The Phase III clinical trials for orteronel and galeterone were halted due to a lack of therapeutic benefits outweighing those of the current medications in the clinic for these agents [31–34]. Seviteronel on the other hand, is presently undergoing Phase II clinical trials for both prostate and breast cancer [23,31]. Pharmacodynamics data for seviteronel has revealed that this drug is a selective 17,20-lyase inhibitor [25,24]. *In vitro* experimental data has revealed a half maximal inhibitory concentration (IC_{50}) of 670 and 69 nM for 17 α -hydroxylase and 17,20-lyase inhibition, respectively [23].

Prospective computational design of novel compounds has enabled the ability to explain the interactions at molecular level and to predict biological activities of novel molecules from their structural properties prior to laboratory testing [31]. Purushottamachar et al. [32] performed a qualitative 3D pharmacophore model for well-known natural AR down-regulating agents, which was subsequently followed by a database search and synthesis of potential AR inhibitors. Furthermore, Gianti et al. [5] used induced-fit docking on CYP17A1 inhibitors on a homology model of CYP17A1, since the X-ray crystal structure of the CYP17A1 enzyme was unavailable. In 2012, two crystal structures of CYP17A1 co-crystallized with CYP17 inhibitors ABT (3RUK) and galeterone (3SWZ) were deposited into the Protein Data Bank (PDB) [23]. This has paved the way for prospective computational design of new inhibitor drugs. However, the absence of cytochrome b5 bound to

CYP17A1 enzyme in current PDB structures still limits modeling the effects of 17,20-lyase inhibition [19,20,21]. Recently, a virtual screening work-flow combined with density functional theory (DFT) and docking on the CYP17A1 structure (3SWZ) was used to identify two potential inhibitors for the CYP17A1 enzyme; however, the downside was that a further inhibition assay revealed that they were not selective to the 17,20-lyase route [33].

There is a great need for third generation antiandrogens that are selective 17,20-lyase inhibitors to treat mCRPC. The main idea is to design drugs that would improve the survival rates of ~5 months that is offered by current medications to 2–5 years. In this work, pharmacophore modelling from non-steroidal CYP17A1 inhibitors was used as a ligand-based drug design (LBDD) approach, as a concrete form of molecular characteristics (spatial distribution of groups) that are essential for molecular realization of a ligand by a protein, receptor or enzyme [32,35,36]. The subsequent pharmacophore hypothesis was further used for a database screening and the selection of hit structures with potential inhibitory capability. Density functional theory [37] was then used to deduce their electronic properties. Lastly, molecular docking was used as a structure-based drug design (SBDD) strategy to reveal the binding mode of hit structures in the active site cavity of CYP17A1 enzyme. Therefore, LBDD and SBDD approaches complement each other [38]. The selected hits from these approaches showing good binding to CYP17A1 enzyme were synthesized as new chemical entities (NCEs) and their IC_{50} values against hydroxylase and lyase routes were measured by bioanalytical tests employing ultra high performance liquid chromatography-tandem mass spectrometry (UHPLC-MS/MS).

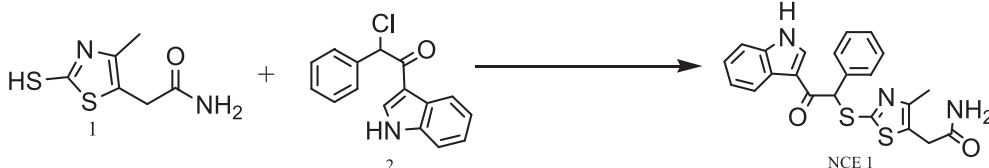
The hypotheses used in this work are the following: (i) the development of novel, effective and selective/secure anti-mCRPC compounds is a constant necessity. Thus, chemical scaffolds different from the currently used in the clinic (with reduced success up to now) are needed. They could be obtained combining *in-vitro* information on non-steroidal inhibitors with computer aided drug design methods (pharmacophore model, database screening, molecular docking for hit selection) (ii) Selective CYP17A1 17,20-lyase inhibitors should not be based on homology models (due to the absence of the important amino acids in the active site of the enzyme at molecular level [39,40]). Thus, the use of available 3RUK and 3SWZ structures are preferable. The one showing best results with its co-crystallized ligands should be selected. (iii) In a preliminary study of novel scaffolds, as in this case, the primary objective is to find compounds showing high selective or virtually specific inhibition of the lyase route (i.e. with null inhibition of the hydroxylase route).

2. Results and discussion

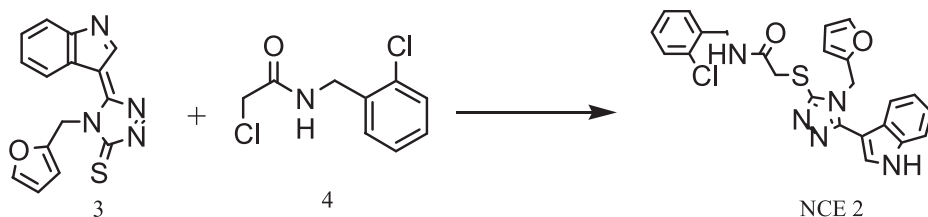
2.1. Chemistry

Herein, we report, for the first time, the synthesis of 13 NCEs based on the scaffolds depicted in scheme 1 to 9. The general procedures for the laboratory synthesis for compound 1-8e as shown in Table 2 is outlined.

The synthesis of NCE 1 was performed by the addition of 2-(2-Mercapto-4-methyl-thiazol-5-yl)-acetamide (compound 1) to a mixture containing 2-Chloro-1-(1H-indol-3-yl)-2-phenyl-ethanone (compound 2) in N,N-Diisopropylethylamine (Hünig's base) and Dimethylformamide (DMF) solvent. A yield of 20% was obtained for NCE 1.



Scheme 1. Reagents and conditions: (1) DMF, DIPEA, 3 hrs, 100 °C, 20%.



Scheme 2. Reagents and conditions: (1) DMF, DIPEA, 3 hrs, 100 °C, 20%.

The synthesis of NCE 2 was performed by adding 4-Furan-2-ylmethyl-5-indol-3-ylidene-[1,2,4]triazolidene-3-thione (compound 3) to a mixture containing 2-Chloro-N-(2-chloro-benzyl)-acetamide (compound 4) in *N,N*-Diisopropylethylamine (Hünig's base) and Dimethylformamide (DMF) solvent. A yield of 20% was obtained for NCE 2.

Commercially available 2-Cyano-N-(4-ethyl-phenyl)-acetamide (compound 5) was reacted with 6-Methoxy-4-oxo-4H-chromene-3-carbaldehyde (compound 6) in a solution containing acetic acid and sodium acetate. Coupling of the two compounds via *N*-acylation and subsequent rearrangements of the amine. Crystallization of the resulting precipitate with acetonitrile gave a 48% yield of the tautomer of NCE 3.

The synthesis of NCE 4 was performed by coupling 2-Amino-3-methyl-benzoic acid (compound 7) with 4-(2-Bromo-ethoxy)-benzene-sulfonamide (compound 8) in *N,N*-Diisopropylethylamine (Hünig's base) and Dimethylformamide (DMF) solvent. A yield of 50% was obtained.

The *N*-acylation of *m*-aminophenyl-2-methoxypropanamide (compound 9) and benzylchloridemethanamide (compound 10) was undertaken by the addition of Hünig's base *N,N*-Diisopropylethylamine (DIPEA) and potassium iodide as a catalyst. The resulting NCE 5 was obtained in 30% yield.

The synthesis of NCE 6 was performed by a coupling reaction of 1H-Indazole-3-carboxylic acid (compound 11) with *N*-[4-(2-Chloro-propionyl)-phenyl]-butyramide (compound 12), by using *N,N*-Diisopropylethylamine (Hünig's base) and Dimethylformamide (DMF) solvent. A yield of 50% was obtained.

Synthesis of NCE 7 was performed by using a commercially available 4-oxo-bis-benzoic acid (compound 13) as a starting material; and was added to a solution containing Tetrahydrofuran (THF), triethylamine, and *t*-butylchloroformate. To the resulting solution 4-aminoisobutyric acid (compound 14) was then added and NaOH in cold water for heterocyclization and *N*-acylation. Then recrystallization of the resulting precipitate yielded 91% of NCE 7.

The synthesis of NCE 8 was performed by reacting [(6-hydroxy-3-oxo-3,4-dihydro-benzoxazin)-7-amine with the commercially available (3-formyl)pyridin-3-ylbenzamide compound 16b was performed in anhydrous ethanol. The reaction starts with reductive amination, followed by the reduction of the imine product that forms. The reaction was allowed to stand overnight at room temperature and purification was performed to yield 74–92% of compound 8, 8a–8e.

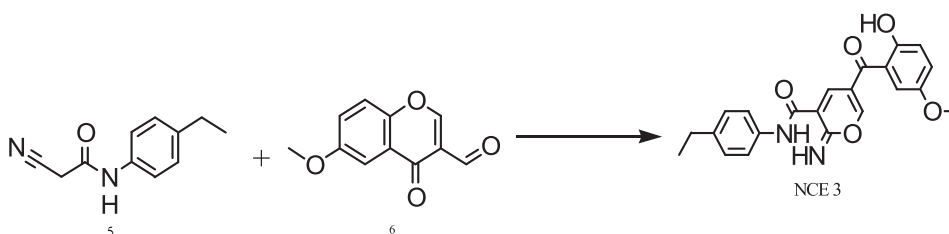
The synthesis of NCE 8d was performed in 2 steps. The *N*-acylation reaction of compound 15c with readily available starting compound 17 was performed by adding the two reagents in anhydrous dichloromethane and triethylamine. This then gave 99% yield of NCE 8d.

2.2. Design of the 3D-pharmacophore model

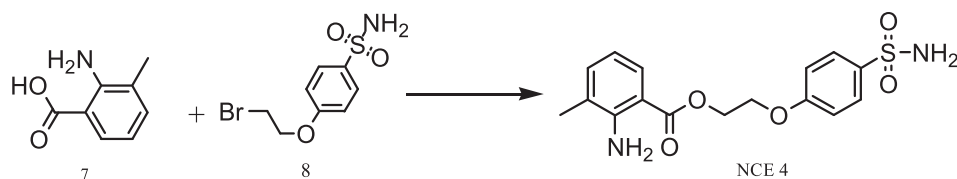
Table 1 shows the 78 studied inhibitors of CYP17A1 enzyme with *in vitro* experimental IC_{50} collected from the literature [2,9,13,19,28,41–43]. The 12 highest active training compounds in Table 1 (ID 1, 2, 4, 7, 9–16) were used to define the CPHs. This data set includes the non-steroidal drug orteronel (TAK700; ID 10), which has been suggested as a lyase inhibitor [9,27]. 36 different six-point common pharmacophore hypotheses (CPHs) were generated by PHASE (Table S1 in Supporting Information shows 12 CPHs including the best one selected). A 3D-QSAR pharmacophore model was generated for each CPH by using all the training compounds in Table 1. All the models were statistically significant (p -values $\ll 0.05$), indicating their reliability [44]. The best CPHs (AADDRR.860; No. 12 in Table S1) was selected according to their best overall predictive ability considering all the compounds in Table 1 ($R^2 = 0.92$, for training, and $Q^2 = 0.89$, for test compounds, using a 3 latent variables-PLS 3D-QSAR model; see other statistics in Table S1).

Fig. 1 shows the estimated ($epIC_{50}$) vs. actual (pIC_{50}) data for all training and test subsets in Table 1 for the 3D-QSAR model based on the best CPH. As can be seen, good agreement between estimated and actual pIC_{50} values is observed, particularly for the most potent compounds (with high pIC_{50}), which are of higher interest. It should be indicated that, originally, 98 compounds were used (including 20 additional steroidal drugs). However, all these extra compounds became outliers (i.e. they did not fit properly the CPHs or were badly predicted by PLS), and were discarded. Only the compound ID 31 in Table 1, an AA analogue, was not an outlier, and was retained for calculations. It was the only unique steroidal compound used in this work.

Table 1 shows the number of pharmacophore sites matched by each molecule as well as the fitness scores (matching degree between the molecule and the best CPH). The molecule ID = 7 in Table 1, with the highest fitness score (3.0), was selected as the reference compound. Fig. 2 shows the reference compound (IUPAC name: *N*-(4'-[1-hydroxy-1-(1H-imidazol-4-yl)-2-methylpropyl][1,1'-biphenyl]-3-yl)acetamide) mapped onto the best CPH. It shows the best CPH features, including two hydrogen bond acceptors (A1 and A3), two hydrogen bond donors (D4 and D5) and two aromatic rings (R10 and R11). It also shows the point vectors giving the direction where the amino acid residues of the enzyme will more likely form hydrogen bonds with the ligand when bound to the target enzyme in its active site; identifying the important characteristic features [45]. The reference molecule shows that the point vector for the hydrogen bond acceptor (A3) is mapped onto the carbonyl group of *N*-methyl-2-carboxamide. The hydrogen bond acceptor vector (A1) is mapped onto the nitrogen of the imidazole ring. The hydrogen bond donor (D4) is mapped onto the OH group of the



Scheme 3. Reagents and conditions: (1) acetic acid, sodium acetate, 100 °C for 8hrs, 48%.



Scheme 4. Reagents and conditions: (1) DMF, DIPEA, 1hr. (2) 6hrs at 100 °C, 50%.

benzanol moiety of the reference molecule. While the hydrogen bond donor vector (D5) is mapped onto the N-H group of N-methyl-2-carboxamide moiety. The naphthalene rings (R10) and (R11), respectively are properly aligned on the position where π - π interactions are most likely to occur with aromatic rings of the amino acids of the enzyme.

2.3. Pharmacophore database screening results

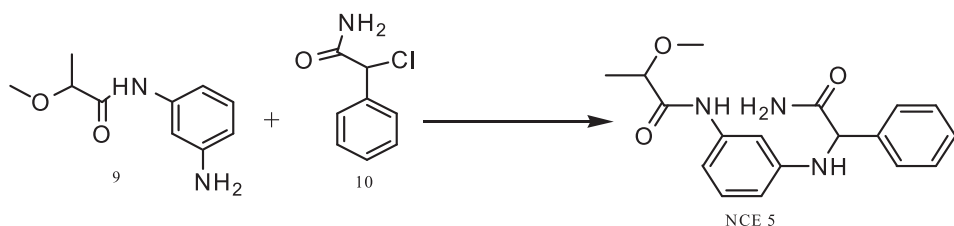
2.5 million structures from the enamine database were evaluated. Those with undesirable functional groups (from a toxicity point of view) and not satisfying the Lipinski's rule of five were removed, reducing their number to 1 million. The predicted activities, estimated from the 3D-QSAR model, provided 798 hit structures with $\text{epIC}_{50} > 7$ having the 6 pharmacophore sites of the best CPH. From them, the VSW provided a set of 20 hit structures, which were submitted to geometry optimization using DFT and further docking study. Eight hit structures, which were finally synthesized, are shown in Table 2 (Namely: 1–8).

2.4. Density functional theory results

DFT calculations were also used to determine the electronic features of the hits. As an example, Fig. S1 (in Supporting Information) shows the results for NCE 1. HOMO and LUMO explains drug-receptor (electrons donating and accepting groups, respectively) interactions as well as reactive (electrophiles or nucleophiles, respectively) functional groups distribution [46]. The HOMO and LUMO spheres, mapped onto the (1H-indol-3-yl)-2-oxo and [2-(1H-indol-3-yl)-2-oxo-1-phenylethyl] moieties, respectively, indicate the ability of NCE 1 to donate and accept electrons, respectively, to appropriate amino acid residues of the receptor. The energies observed for HOMO (−0.220 eV) and LUMO (−0.056 eV) orbitals shows a small difference, which indicates that NCE 1 is reactive [47,48]. The HOMO-LUMO energy differences for all the hits were in the range of 0.111 to 0.185 eV, indicating their reactivity.

The molecular electronic density shows two regions of low electronic density: the NH group of the indole moiety as the hydrogen bond donor, and the NH_2 groups of the acetamide moiety, as well as a region of high electronic density corresponding to electronegative carbonyl groups (of the oxo and acetamide moieties). The MESP indicates the most electronegative functional groups (the carbonyl groups of the phenyl-2-oxo and acetamide moieties, the N atom of the thiazole moiety), as well as the least electronegative part (ring system). The obtained isovalue of −57.380 kcal/mol for MESP mapped on NCE 1 after geometry optimization is shown in Fig. S1.

All of the electronic properties obtained by (DFT) indicate the reactive site of the hits in relation to the selected AADRR860 3D-QSAR pharmacophore model and the relationship between the structures and their reactivity.



Scheme 5. Reagents and conditions: (1) DIPEA, potassium iodide (catalyst), DMF, boiling water bath for 5 min (2) 6hrs at 100 °C, 30%.

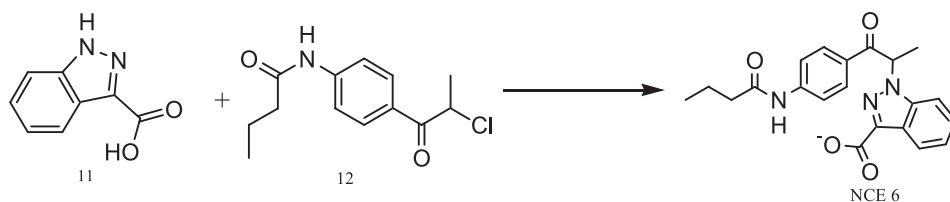
2.5. Molecular docking results

The PDB enzyme structure 3SWZ was selected over 3RUK for further docking studies because of its lower resolution and the consistent docking score and RMSD results, for both, IFD and cross-docking stages (see Table S2 in Supporting Information). The galeterone (TOK001) pose estimated by IFD docking was superimposed over the co-crystallized structure of TOK001 in 3SWZ as a way to verify the performance of the docking process [49]. A high degree of overlap between the two structures was found (see Fig. S2 in Supporting Information).

The 20 optimized hit structures were submitted to molecular docking. As an example, Fig. S3 (in Supporting Information) shows the resulting pose from IFD and the ligand interaction diagram (LID) of NCE 1. The binding mode for NCE 1 is an example of type I inhibition, characterized by the absence of metal coordination between the indole N-heterocyclic moiety and Fe^{3+} of ferric heme [25]. Type II inhibition is characterized by a metal coordination between Fe^{3+} of the enzyme and the N-heterocycle of the ligand. Instead, in NCE 1 there is a π - π interaction between the indole moiety of the molecule and the porphyrin moiety of ferric heme of the enzyme (see Fig. S3B). In addition, there are three hydrogen bonds between: the NH group of the indole ring moiety and the carbonyl group of VAL482, the NH group of the acetamide moiety and the carbonyl group of ASN202, and the carbonyl group of the acetamide moiety and the NH group of ARG239. Finally, hydrophobic interactions involved in this binding event includes (the involved CYP17A1 enzyme residues, in green color, are shown in Fig. S3B). The relevant functional groups that are predicted by DFT (Fig. S1; Supporting Information) are in agreement with the functional groups involved in hydrogen bonding and π - π interactions with the CYP17A1 enzyme by molecular docking (Fig. S3; Supporting Information).

The binding mode for NCE 1 is similar to the binding mode of endogenous substrates of CYP17A1 enzyme such as pregnenolone, progesterone, 17 α -hydroxypregnenolone, and 17 α -hydroxyprogesterone. These endogenous substrates undergo type I inhibition, where an active site water as a sixth ligand is displaced from the heme coordination during the catalytic cycle [19,25,40,50]. On the contrary, the binding mode of NCE 1 is different from the binding mode observed for TOK001 and ABT [23], which shows type II inhibition, where their metal binding groups undergoes metal coordination with ferric heme. NCE 1 also shows a hydrogen bond between its OH group and the carbonyl group of ASN202 [50]. This interaction is also observed in the binding mode found here for TOK001 (see Fig. S2B in Supporting Information).

After visual inspection of the poses for the NCEs on the enzyme cavity of 3SWZ, it was decided to select 12 NCEs (satisfying the filtering criteria) as well as some derivatives from the skeleton of one NCE. Only the synthesis of structures shown in Table 2 as new chemical entities (NCEs) was feasible. They include eight NCEs (1–8) and five derivatives from the skeleton of NCE 8 yielding (NCEs 8a to 8e).



Scheme 6. Reagents and conditions: (1) DIPEA, DMF, 100 °C for 1 hr (2) 100 °C for 6 hrs, 50%.

2.6. Biological activities

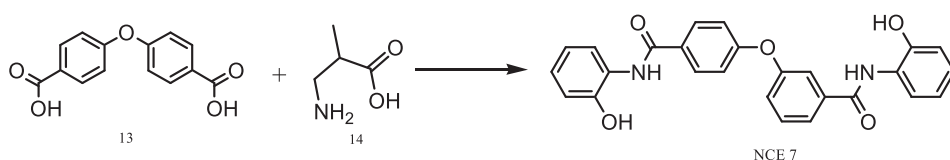
The NCEs in Table 2 were investigated as possible inhibitors of the 17 α -hydroxylase and lyase activities of human CYP17A1, using pregnenolone and 17 α -hydroxypregnenolone as substrates, respectively. Chromatograms for the corresponding measured metabolites (17 α -hydroxypregnenolone and DHEA, respectively) and the IS (imipramine) are shown in Fig. S4 in the Supporting Information. It is difficult to judge and compare the IC_{50} values of novel inhibitors because of the differences in the experimental conditions of assays. For instance, the inhibition of the hydroxylase route of AA has provided *in vitro* IC_{50} values ranging from 1.7 nM [13] to 201 nM [23]. Furthermore, in the literature different substrates have been used such as pregnenolone [13] and progesterone [23] in the assays for CYP17A1 inhibition. Our hydroxylase v.s. lyase assay uses human CYP17A1 extracted from *E. Coli*. Whereas in the literature some authors have used CYP17A1 enzymes extracted from mammalian species such as adrenals and mammalian cells expressing CYP17A1 and Cytochrome b5 [24]. Accordingly, the IC_{50} 's obtained in this work will differ significantly in contrast to literature data due to heterogeneous experimental assay. Thus, the use of negative and positive control inhibitors (e.g. ketoconazole and AA, respectively) has been suggested for comparison purposes [19,25,50]. In this work, AA was assayed, in parallel to the NCEs under study, as a positive control inhibitor in the CYP17A1 hydroxylase and lyase assay, respectively. Table 3 shows the half-maximal inhibitory concentrations (IC_{50} -values in μ M units) determined for the NCEs and AA, as well as literature results for AA for comparison [13,19,33,50–52]. Individual dose-response curves can be found in the supporting information (Table S3). As can be observed, IC_{50} -values for AA are reasonable comparable to those in the literature; which validate the method used. NCEs with $IC_{50} > 160 \mu$ M were considered to provide null inhibition.

NCE 1 shows partial inhibitory activity at mid- μ M level for hydroxylase and lyase routes (IC_{50} of 80.5 and 32.9 μ M, respectively). Unfortunately, it was synthesized as a racemic mixture (due to experimental difficulties related to asymmetric synthesis and optical resolution methods), instead of synthesizing the (R)-enantiomer as suggested by resulting docking pose (Fig. S3B; Supporting Information). Regarding the synthesized derivatives, only NCE 8a and 8c showed inhibitory activity at mid- μ M level for CYP17A1 lyase inhibition. NCE 8a showed null inhibition and $IC_{50} = 61.4 \mu$ M for hydroxylase and lyase inhibition, respectively (a very important combination in terms of selectivity/security of an anti-mCRPC drug). The real interest of Table 3 is to explore the lyase:hydroxylase selectivity (as the IC_{50} -hydroxylase / IC_{50} -lyase ratio). NCEs 1 and 8c shows noticeable selectivity (around 2.5) while 8a shows a high selectivity, becoming virtually specific for the lyase route. In contrast to NCE 8a, for NCEs 7, 8 and 8d, the value of IC_{50} for the lyase inhibition is too close to the limit (160 μ M) and their selectivity becomes *a priori* poor. As before, the selectivity result for AA in this work (2.1) is reasonable comparable to some favorable

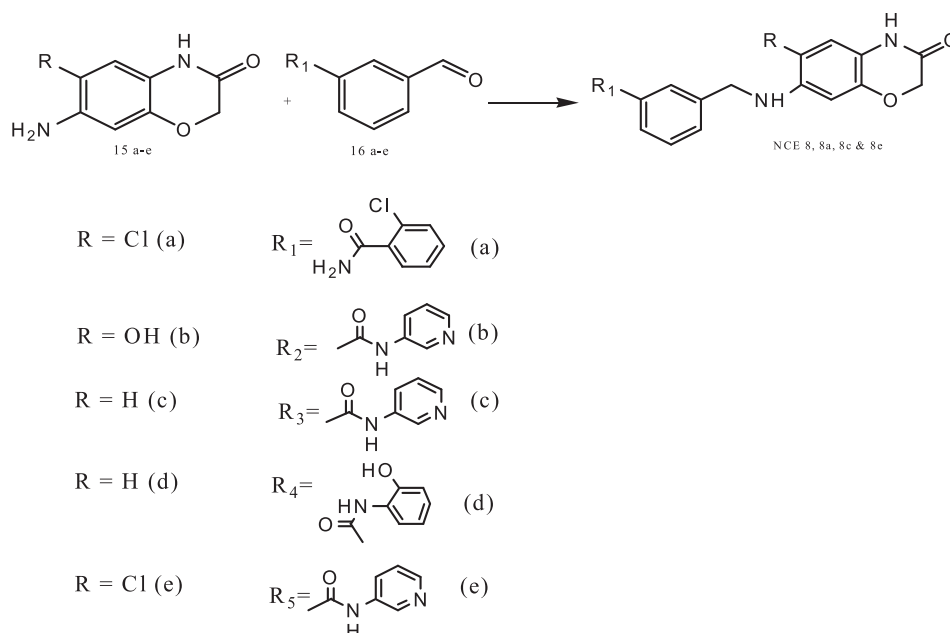
selectivity data to lyase route reported previously (validating the methodology). The selectivity data for AA is comparable to that of our compounds in Table 3. Even though the selectivity of NCE 1 and 8c is more lyase specific than AA. [24]. The reported IC_{50} values for hydroxylase:lyase inhibition of TOK001 are 73 & 23 nM, respectively. The selectivity of TOK001 is thus, 3.1 and is partially favourable towards the lyase route [24]. Therefore, the clinical data has pointed out that TOK001 is a lyase inhibitor. Even though the clinical trials for TOK001 has been halted. Since, there are no observed therapeutic benefits of TOK001 that outweighs those of AA [31–34]. The selectivity of 3.1 is confirmed by this clinical observation, which means that a high selectivity gives rise to full lyase inhibition. Whereas the reported IC_{50} values for VT-464 are 670 and 69 nM, respectively [23,31]. Therefore, the observed selectivity of 9.8 for VT-464 is skewed towards the lyase route. There is a body of evidence supporting the claim that the selectivity of VT-464 is favourable towards the lyase route. Bird et al. has also pointed out that pre-clinical data using non-human primates off-target interactions such as MES were suppressed, which has led to the clinical trials to be undertaken without co-administration of VT-464 with prednisone [24]. Therefore, a selectivity of 9.8 proves that VT-464 is a true selective lyase inhibitor. The compounds identified in this work (i.e. NCE 1 and 8c) can be optimized more in order to attain nM inhibition and a selectivity greater than 10, suggesting that this would lead to new compounds identified by this work.

An explanation for the selectivity of NCE 1 over other NCEs could be attributed to the presence of the indole moiety of the ligand as well as the acetamide moiety. For 8a, the unique lyase activity could be attributed to the inclusion of an OH group in R_1 as well as the presence of N-(pyridin-3-yl)acetamide heterocycle (see Table 3). The superior lyase inhibitory potency over the hydroxylase of NCE 8c could be attributed to the inclusion of N-(2-hydroxyphenyl)acetamide heterocycle to the core-structure (see Table 3). This is consistent with the observations made by Bonomo et al.[33], who indicated that the presence of N-heterocycles on the ligand when it binds with the CYP17A1 enzyme improves the binding affinity. In contrast, the chloro group in either R_1 or R_2 on the skeleton structure of the derivatives seems to reduce IC_{50} values for both lyase and hydroxylase activities (see Table 3).

It is difficult (but desirable) to try to connect docking outputs to experimental values, and just hypothesis can be defined. Such hypothesis could be used to plan further optimization stages. As a hypothesis, in the case of NCE 8a, the introduction of an OH group as R_1 in the skeleton of hit 8 (not present in other derivatives of Table 2) could be related to the high lyase selectivity. Docking outputs revealed that this OH group forms simultaneously two hydrogen bonds (ARG239 and ASP298 residues; Fig. S5 in Supporting Information). Also, as hypothesis, in the case of NCE 8c, the introduction of the N-(2-hydroxyphenyl)acetamide group in the skeleton of hit 8 (not present in other derivatives of Table 2) could be related to the lyase selectivity. Docking outputs indicates a strong hydrogen bond between the OH group of N-(2-hydroxyphenyl) as the hydrogen bond donor and the carbonyl group



Scheme 7. Reagents and conditions: (1) THF, triethylamine, *t*-butylchloroformate, –78 °C. (2) NaOH, THF, 2 hrs, 91%.



Scheme 8. Reagents and conditions: (1) methanol, 58–60 °C for 60–90 min. (2) acetonitrile, sodium borohydride, 0 °C. (3) sonication for 2 hrs at room temperature. (4) stand overnight at room temperature, 74–92%. Where: (a) NCE 8, (b) NCE 8a, (c) NCE 8b, (d) NCE 8c, and (e) NCE 8e.

of VAL482 as the hydrogen bond acceptor Fig. S6 in Supporting Information), with a bond radius of 1.61 Å (the strongest interaction found for NCEs in Table 2).

The IC_{50} values of NCE 1, 8a and 8c (μM level) are higher than those for the control are (ABT; nM level). However, compared to this control, these three NCEs present a higher selectivity value (Table 3) with the method used in this work. These results are adequate enough to consider these NCEs as leads compounds for further optimization to yield nM lyase inhibitors. In our opinion, such novel chemical scaffolds could be useful to design drugs that do not succumb to MES (due to hydroxylase route inhibition), as occurs with ABT. Particularly, NCE 8a seems to be ineffective to inhibit the hydroxylase route according to the current experimental conditions (Table 3), which is the most promising fact.

Further strategies to optimize the three promising NCEs found could include the following: (i) to separate the R and S enantiomers and measure their hydroxylase and lyase inhibition. (ii) to synthesize and test the tentative structures of major metabolites of the NCEs; that could be obtained by the Phase I & II metabolism of them on human hepatocytes. The tentative structures of the major metabolites could be elucidated from UHPLC-MS/MS experiment. The aim would be to evaluate their binding to CYP17A1 enzyme in the hydroxylase and lyase routes by the proposed method; (iii) to design derivatives of these NCEs by altering their functional groups using R group enumeration panel on Schrödinger suite and free energy perturbation (FEP+) [53]; (iv) to perform hit expansion, bioisostere replacement/addition and further relative binding affinity prediction with (FEP+) [53–57]. FEP+ essentially works by predicting the relative binding affinities of compounds with known IC_{50} values obtained in similar experimental conditions.

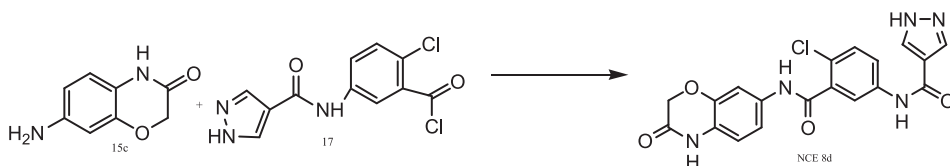
3. Conclusions

A 3D-QSAR pharmacophore model was able to predict, with a reliability level of 90% (predictive ability), the inhibitory activity of 78 CYP17A1 non-steroidal inhibitors sourced from the literature (with diverse *in vitro* IC_{50} data and chemical classes). The optimum pharmacophore hypothesis has two hydrogen bond acceptors, two hydrogen bond donors and two aromatic rings groups. They represent non-steroidal structures but not steroidal ones. It allowed screening 2.5 million structures to get the best hits. Density functional theory and docking calculations provided clues on the structure-activity relationships and binding modes. Eight highly active hits, plus five derivatives of one of them, were synthesized as new chemical entities (NCEs). *In vitro* IC_{50} values for the CYP17A1 hydroxylase and lyase inhibition routes demonstrated selectivity to the lyase route of three NCEs (better than abiraterone). One of them showed null inhibition for the hydroxylase route (indispensable to avoid the undesirable use of prednisone). They still fail in *in vitro* inhibitory activity (μM level). However, they should serve as starting point of designing/optimizing/synthesizing new potent selective CYP17A1 17,20-lyase inhibitors based on different chemical scaffolds from the currently used in the clinic (with reduced success up to now). Such strategy could offer alternative potential therapeutic drugs that could improve the overall survival rates of patients diagnosed with metastatic-castration resistant prostate cancer. Moreover, when the challenge is still to overcome the recent research failures.

4. Experimental section

4.1. Chemistry

General: Melting points were determined on an OptiMelt Automated Melting Point System, Digital Image Processing Technology SRS Stanford



Scheme 9. Reagents and conditions: (1) anhydrous dichloromethane, triethylamine, room temperature for 14 h (2) ethyl acetate, 99%.

Table 1

Non-steroidal compounds (except ID 31) used for pharmacophore modelling.

ID	Name	Class	Subset	Sites matched	Ligand sites	Fitness	IC ₅₀	pIC ₅₀	epIC ₅₀ -3LV
1	3d [28]	1	1	5	A1 A2 D- D3 R7 R6	0.9	13	7.89	7.46
2	1 [41]	2	1	6	A1 A3 D4 D6 R10 R11	1.0	16	7.80	7.45
3	5 [43]	3	2	4	A- A1 D- D3 R9 R8	1.7	18	7.74	7.55
4	(+)-3c [41]	1	1	6	A1 A3 D4 D5 R9 R8	0.8	19	7.72	7.61
5	13 [43]	3	2	4	A- A1 D- D3 R10 R9	1.7	19	7.72	7.50
6	24 [43]	3	2	6	A1 A3 D4 D5 R11 R12	3.0	21	7.68	7.67
7 ^a	17 [43]	3	1	6	A1 A3 D4 D5 R10 R11	3.0	24	7.62	7.70
8	15 [43]	3	2	4	A1 A- D3 D- R9 R10	2.0	27	7.57	7.38
9	16 [43]	3	1	4	A1 A- D3 D- R9 R10	2.0	28	7.55	7.37
10 ^b	TAK700 [28]	4	1	5	A1 A3 D5 D- R12 R13	0.9	28	7.55	7.81
11	3b [28]	1	1	6	A1 A3 D4 D5 R10 R9	1.1	29	7.54	6.98
12	7 [43]	3	1	4	A1 A- D3 D- R8 R9	2.0	33	7.48	7.48
13	26 [43]	3	1	6	A2 A4 D5 D6 R11 R12	2.6	36	7.44	7.57
14	16 [43]	3	1	4	A- A2 D- D5 R9 R8	1.5	37	7.43	7.12
15	32 [43]	3	1	6	A1 A3 D4 D5 R8 R9	2.6	38	7.42	7.4
16	33 [43]	3	1	6	A1 A3 D4 D5 R9 R10	2.9	40	7.40	7.54
17	22 [43]	3	1	6	A1 A3 D4 D5 R10 R11	2.5	44	7.36	7.45
18	34 [43]	3	2	6	A1 A3 D4 D5 R10 R9	2.6	45	7.35	7.36
19	14 [43]	3	1	4	A- A1 D- D3 R10 R9	1.7	49	7.31	7.44
20	9 [9]	5	1	4	A- A2 D- D5 R7 R6	1.5	52	7.28	7.16
21	9a [9]	5	1	3	A- A3 D- D- R7 R8	1.4	52	7.28	7.17
22	26 [2]	4	1	4	A- A2 D- D5 R7 R6	1.5	52	7.28	7.16
23	8 [43]	3	1	5	A1 A3 D4 D- R11 R10	1.1	54	7.27	7.13
24	13 [2]	4	1	3	A- A- D- D3 R7 R6	2.0	56	7.25	7.15
25	20 [28]	1	1	3	A- A- D3 D- R6 R7	1.2	64	7.19	7.43
26	6 [19]	6	2	5	A1 A3 D6 D- R15 R16	1.0	69	7.16	6.95
27	15 [2]	4	1	3	A- A- D3 D- R7 R8	1.2	75	7.12	7.43
28	22 [2]	4	1	3	A- A- D- D5 R9 R8	2.0	75	7.12	7.07
29	36 [43]	3	1	6	A1 A3 D4 D5 R8 R9	1.6	77	7.11	6.74
30	3i [28]	1	2	6	A1 A3 D4 D5 R12 R11	0.7	88	7.06	7.13
31 ^c	8 [9]	7	1	3	A- A- D- D3 R5 R6	1.8	97	7.01	7.02
32	24 [2]	4	1	3	A- A- D- D3 R5 R4	1.8	97	7.01	7.02
33	18 [41]	3	1	5	A1 A- D4 D5 R10 R11	1.8	120	6.92	7.06
34	6 [43]	3	1	5	A1 A3 D4 D- R11 R10	1.3	130	6.89	7.01
35	19 [28]	1	1	4	A- A3 D- D4 R8 R7	1.5	144	6.84	6.65
36	25 [43]	3	1	4	A2 A- D4 D- R10 R9	2.0	150	6.82	7.37
37	23 [43]	3	1	6	A1 A2 D5 D6 R11 R12	2.3	160	6.80	7.02
38	5ax [42]	8	1	4	A1 A- D2 D- R6 R5	1.4	170	6.77	6.77
39	2c [19]	6	2	4	A3 A2 D- D5 R12 R-	1.3	180	6.74	7.17
40	10 [9]	5	1	3	A- A- D- D3 R6 R5	1.5	186	6.73	6.66
41	14 [13]	9	1	3	A- A- D- D3 R7 R6	1.5	188	6.73	6.62
42	25 [2]	4	1	3	A- A- D- D3 R6 R5	1.5	186	6.73	6.80
43	3e [28]	1	1	6	A1 A3 D4 D5 R10 R9	0.7	190	6.72	6.61
44	11 [2]	4	1	3	A- A- D- D3 R6 R5	2.1	189	6.72	6.60
45	27 [2]	4	2	3	A- A- D- D2 R5 R4	2.0	226	6.65	6.71
46	30 [43]	3	1	3	A1 A- D- D- R7 R6	1.6	236	6.63	6.48
47	5ay [42]	8	1	3	A1 A- D2 D- R- R7	1.6	240	6.62	6.52
48	4 [9]	5	2	3	A- A- D- D3 R5 R6	1.4	248	6.61	6.71
49	5bx [43]	8	1	4	A1 A- D2 D- R6 R5	1.4	250	6.60	6.41
50	31 [43]	3	1	3	A1 A- D- D- R6 R5	1.7	263	6.58	6.45
51	3f [28]	1	2	6	A1 A3 D4 D5 R9 R10	0.5	290	6.54	6.62
52	13 [28]	1	1	4	A- A3 D- D4 R8 R7	1.5	307	6.51	6.65
53	2 [28]	1	1	4	A1 A- D3 D- R6 R8	1.1	333	6.48	6.27
54	28 [2]	4	1	3	A- A- D- D3 R7 R6	2.0	337	6.47	6.67
55	14 [2]	4	1	3	A- A- D- D3 R7 R6	1.4	343	6.46	6.60
56	27 [43]	3	2	3	A1 A- D- D- R5 R4	1.5	373	6.43	6.34
57	3g [28]	1	1	6	A1 A3 D4 D5 R10 R9	0.7	400	6.40	6.56
58	3j [28]	1	1	6	A1 A3 D4 D5 R8 R9	0.9	410	6.39	6.5
59	6 [28]	1	1	3	A2 A- D- D- R7 R9	1.6	423	6.37	6.25
60	25 [9]	5	1	3	A- A- D- D3 R5 R4	1.3	438	6.36	6.59
61	5 [28]	9	1	3	A2 A- D- D- R6 R8	1.6	587	6.23	6.21
62	29 [43]	3	1	3	A1 A- D- D- R6 R5	1.6	584	6.23	6.35
63	KTZ [2]	10	1	4	A3 A5 D- D- R10 R11	1.1	740	6.13	5.99
64	23 [9]	5	1	3	A- A- D- D2 R5 R4	1.5	760	6.12	6.33
65	12 [2]	4	1	3	A- A- D- D3 R6 R5	1.9	783	6.11	6.44
66	12 [9]	5	1	5	A3 A2 D- D4 R6 R5	2.1	876	6.05	6.13
67	28 [43]	3	1	3	A1 A- D- D- R5 R4	1.5	953	6.02	6.3
68	17 [9]	5	1	4	A3 A- D4 D- R6 R7	1.4	1370	5.86	5.94
69	13 [9]	5	2	4	A2 A- D4 D- R5 R6	1.6	1790	5.75	6.16
70	24 [9]	5	1	3	A2 A- D- D- R6 R5	1.2	2000	5.7	5.50
71	8 [28]	1	1	3	A1 A- D- D- R5 R6	1.1	2346	5.63	5.65
72	16 [9]	5	1	3	A2 A- D- D- R7 R6	1.1	3340	5.48	5.26
73	7 [28]	1	2	4	A3 A- D- D4 R10 R8	1.2	5000	5.3	6.02
74	10 [28]	1	1	3	A2 A- D- D- R7 R6	1.2	5000	5.3	5.19

(continued on next page)

Table 1 (continued)

ID	Name	Class	Subset	Sites matched	Ligand sites	Fitness	IC ₅₀	pIC ₅₀	epIC ₅₀ -3LV
75	4 [28]	1	1	4	A3 A- D- D4 R10 R8	1.1	10,000	5.00	5.02
76	1 [28]	1	1	4	A1 A- D3 D- R6 R8	1.7	20,000	4.7	4.93
77	3 [28]	1	2	4	A3 A- D- D4 R9 R7	1.2	20,000	4.7	5.09
78	15 [28]	1	1	3	A1 A- D- D- R5 R6	1.3	20,000	4.7	4.98

^a Reference compound.^b Orteronel.

^c Abiraterone analog (steroidal drug). ID = index. Name = code used in the original paper (reference indicated). Class = chemical family (1: naphthylmethylimidazole; 2: naphthalene-2-carboxamide; 3: biphenylmethylene 4-pyridine; 4: methylene imidazole substituted biaryls; 5: biphenylmethylenes; 6: 4-(1,2,3-triazole); 7: abiraterone analog; 8: imidazolyl and triazolyl substituted biphenyl; 9: biphenylmethylimidazole; 10: Imidazole). Subset = training (1) and test (2) for 3D-QSAR PLS model validation. Sites matched = Number of groups in the molecule fitting the features of the pharmacophore. Fitness = fitness score (matching degree between the molecule and the best common pharmacophore hypothesis). IC₅₀ = half maximal inhibitory concentration. pIC₅₀ = -log(IC₅₀), used as response variable in the 3D-QSAR PLS model. epIC₅₀-3LV = estimated pIC₅₀ value from the PLS model with 3 latent variables. KTZ = ketoconazole (ID 63). The Ligand sites column includes pharmacophore features (letters): hydrogen bond acceptors (A), hydrogen bond donors (D) and aromatic rings (R), with the number of available site points of each type.

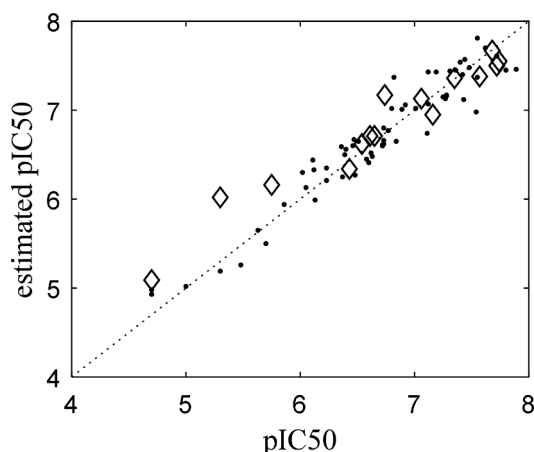


Fig. 1. Validation plot of the 3D-QSAR model based on the best common pharmacophore hypothesis (CPH) showing the estimated versus the actual pIC₅₀ values for the training (dot) and test (diamonds) compounds, subsets 1 and 2, respectively, in Table 1.

Research Systems. NMR spectra were measured on a Bruker Top Spin 3.2 (400 MHz). The solvent used for NMR analysis was CDCl₃ or DMSO-*d*₆ with Tetra Methyl Silane (TMS) as an internal standard. The *J* (coupling constant) values were estimated in Hertz (Hz). Atmospheric pressure chemical ionization (APCI) mass spectra were determined on an Agilent Technologies 1260 Infinity II LC/MSD system with DAD \ELSD G7102A 1290 Infinity II and Agilent LC/MSD G6120B mass-spectrometer. All compounds tested for bioassay had a purity of

95–100%. Abbreviations used are as follows: s = singlet, d = doublet, t = triplet, m = multiplet, br s = broad singlet.

4.1.1. Synthetic protocols

4.1.1.1. General procedure for method A. To a solution of 9.37 mmol of compound **15** in 15 ml of anhydrous ethanol 11.44 mmol of corresponding compound **16** was added at room temperature with stirring. Thin Layer Chromatography (TLC) was used to control the end point of the reaction. The reaction mixture was filtered. The resulting solid was washed with anhydrous ethanol to give 7.665 mmol of yellow solid product that was dissolved in 20 ml anhydrous ethanol. 0.445 g (11.5 mmol, 96%) sodium borohydride was added in portions and stirred for 30 min at room temperature. The reaction mixture was poured into ice water, filtered, dried to give products: **8**, **8a–8e**. The yields were 74–92%.

4.1.1.2. General procedure for method B. To a solution of compound **15** (99 mg; 600 μmol) in anhydrous dichloromethane (2 ml), triethylamine (105 μL, 753 μmol), and compound **17** (170 mg, 600 μmol) in anhydrous dichloromethane (2 ml) were added and the mixture was agitated at room temperature for 14 hrs. Water was added to the reaction solution and an organic phase was extracted with ethyl acetate. The organic phase was washed with water and saturated aqueous solution of sodium bicarbonate and sodium chloride. The resulting mixture was dried over magnesium sulfate followed by concentration under a reduced pressure. A crude product was purified via silica gel column chromatography using hexane:ethyl acetate (1:1) as an eluting solvent yielding **8d** (160 mg, 99%).

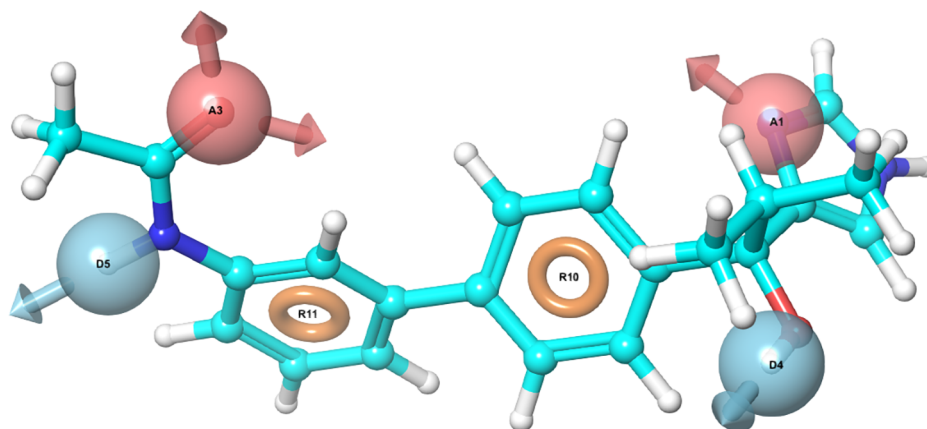
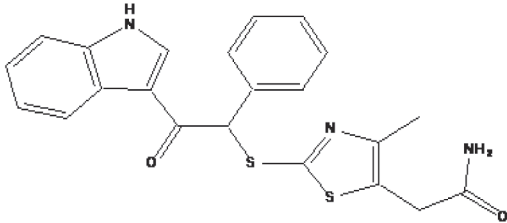
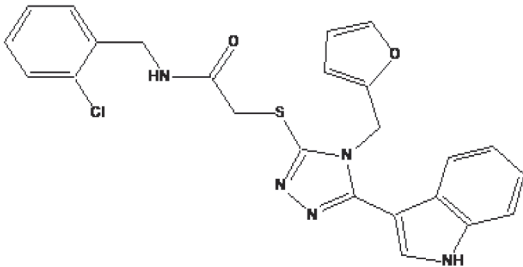
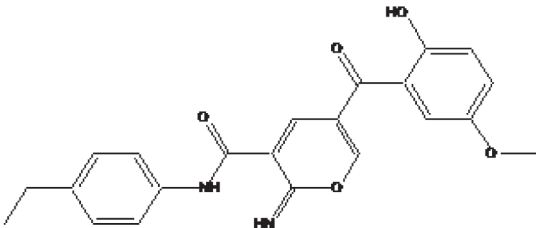
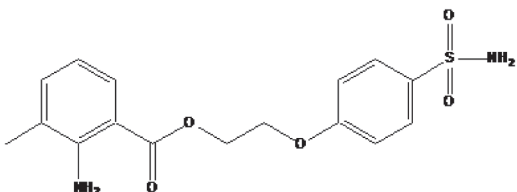
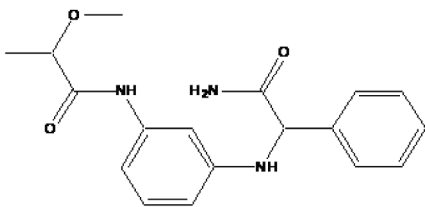
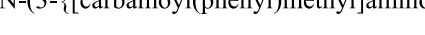


Fig. 2. Pharmacophore model with site point vectors of the best common pharmacophore hypothesis (CPH) mapped onto the structure of the reference compound (ID 7 in Table 1). CPH: AADRR. A = acceptor group; D = donor group; R = aromatic ring.

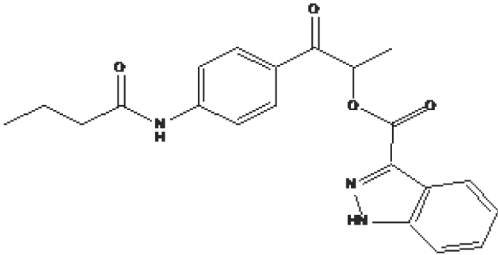
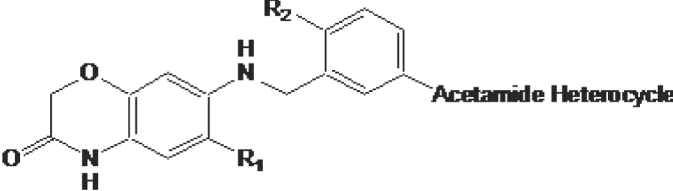
Table 2

Hit structures that were synthesized as new chemical entities (NCEs) with their IUPAC names.

Name	2D Structure and IUPAC name
1	
2	<p>((R)-2-(2-((2-(1H-indol-3-yl)-2-oxo-1-phenylethyl)thio)-4-methylthiazol-5-yl)acetamide)</p> 
3	<p>N-[(2-chlorophenyl)methyl]-2-({4-[(furan-2-yl)methyl]-5-(1H-indol-3-yl)-4H-1,2,4-triazol-3-yl}sulfanyl)acetamide</p> 
4	<p>N-(4-ethylphenyl)-5-(2-hydroxy-5-methoxybenzoyl)-2-imino-2H-pyran-3-carboxamide</p> 
5	<p>2-(4-sulfamoylphenoxy)ethyl 2-amino-3-methylbenzoate</p> 
6	<p>N-(3-{[carbamoyl(phenyl)methyl]amino}phenyl)-2-methoxypropanamide</p> 

(continued on next page)

Table 2 (continued)

Name	2D Structure and IUPAC name
7	 <p>1-(4-butanamidophenyl)-1-oxopropan-2-yl-1H-indazole-3-carboxylate</p>
8	<p>N-(2-hydroxyphenyl)-4-{3-[(2-hydroxyphenyl)carbamoyl]phenoxy} benzamide</p>  <p>Acetamide Heterocycle</p>
8a	<p>R₁ = Cl; R₂ = H Acetamide Heterocycle = N-(pyridin-3-yl)acetamide;</p>
8b	<p>R₁ = OH; R₂ = H Acetamide Heterocycle = N-(pyridin-3-yl)acetamide;</p>
8c	<p>R₁ = H; R₂ = H Acetamide Heterocycle = N-(2-hydroxyphenyl)acetamide;</p>
8d	<p>R₁ = H; R₂ = H Acetamide Heterocycle = 1H-pyrazole-4-carboxamide;</p>
8e	<p>R₁ = H; R₂ = Cl Acetamide Heterocycle = N-(pyridin-3-yl)acetamide;</p>

The molecules **8a** to **8e** are derivatives from the hit **8** skeleton.

4.1.1.3. General procedure for method C. A mixture of 526 mg (2 mmole) 4-oxy-bis-benzoic acid and 3 ml THF and 0.22 ml (2 mmole) triethylamine was cooled in an ultra low temperature freezer and then 0.275 ml (2 mmol) *t*-butylchloroformate was added while stirring. The product was cooled again in a freezer and 390 mg (4 mmol) 4-aminoisobutyric acid and 0.5 g sodium hydroxide in 1 ml cold water was added with 2 ml THF. The solution was stirred for 2 hrs, evaporated, cold water was added, and evaporated again to remove the rest of the THF. The product was recrystallized from isopropanol to give **7** as a white powder (yield 0.6 g; 91%). Physical and spectral data are presented below.

4.1.2. ((R/S)-2-(2-((2-(1H-indol-3-yl)-2-oxo-1-phenylethyl)thio)-4-methylthiazol-5-yl)acetamide) (NCE1).

A vial was charged with 2-(2-Mercapto-4-methyl-thiazol-5-yl)-acetamide (1.0 equiv.), Dimethyl Formamide (DMF) (2 ml), *N,N*-Diisopropylethylamine (DIPEA) (1.2 equiv.). To the stirred mixture 2-Chloro-1-(1H-indol-3-yl)-2-phenyl-ethanone (1.0 equiv.) was added. The vial was capped and heated while stirring for 1hr. After 30 min, the reaction mixture became clear and heating was continued for further 3hrs. Then the vial was cooled, diluted with water, and a precipitate formed was filtered off, washed with water and dried. The average yield was 20%; mp, 202–203 °C; ¹H NMR (400 MHz, DMSO-D₆), δ 2.17 (s,

Table 3

Experimental IC_{50} values (in μM units; mean from duplicate assays) for the synthesized new chemical entities (NCEs) in Table 2 and abiraterone (ABT; positive inhibition control) against human CYP17A1 hydroxylase and lyase routes and lyase:hydroxylase selectivity. For ABT, literature results are also included.

NCE (in Table 2)	IC_{50} -hydroxylase	IC_{50} -lyase	Lyase:hydroxylase selectivity	Reference
1	80.5	32.9	2.4	This work
2	n.i.	*	–	
3	n.i.	n.i.	–	
4	n.i.	*	–	
5	n.i.	n.i.	–	
6	n.i.	n.i.	–	
7	n.i.	141	Poor	
8	n.i.	135	Poor	
8a	n.i.	61.4	High	
8b	n.i.	n.i.	–	
8c	88.8	35.4	2.5	This work
8d	n.i.	156	Poor	
8e	n.i.	n.i.	–	
ABT (positive control)	0.017	0.008	2.1	
	0.0017	0.0153	0.1	
	0.0025	0.015	0.2	
	0.092	0.036	2.6	
	0.004	0.0025	1.6	
	0.025	0.016	1.6	
	0.030	0.027	1.1	
	0.007	0.012	0.6	

* IC_{50} not determined since the inhibition did not decrease with increased inhibitor concentration. n.i.: 160 μM was fixed as the maximum assay concentration (this IC_{50} value was considered as null inhibition, n.i.). The lyase:hydroxylase selectivity was calculated as the IC_{50} -hydroxylase / IC_{50} -lyase ratio.

$-CH_3$), 3.44 (s, 2H, $-CH_2$), δ 6.46 (s, $-CH$), 7.05 (s, 1H, NH_2), 7.16–7.26 (m, 3H, aromatic), 7.30–7.34 (m, 2H, aromatic), 7.44–7.46 (dd, 1H, $^3J = 6.18$ Hz and $^4J = 1.40$ Hz, aromatic), δ 7.54 (s, 1H, NH_2), 7.63–7.65 (m, 2H, aromatic), 8.13–8.15 (dd, 1H, $^3J = 6.99$ Hz and $^4J = 2.26$ Hz, aromatic), 8.71–8.72 (d, 1H, $^3J = 3.15$ Hz, indole-H) and 12.15–12.16 (d, 1H, $^3J = 2.35$ Hz, indole-NH); ^{13}C NMR (100 MHz, DMSO- D_6), δ 15.3, 33.3, 59.0, 112.8, 114.5, 121.7, 122.7, 123.7, 126.1, 126.6, 128.5, 128.9, 129.2, 135.9, 137.1, 137.7, 148.9, 158.7, 170.9, 188.9; MS (APCI): $m/z = 422$ [$M^+ + H$].

4.1.3. *N*-[(2-chlorophenyl)methyl]-2-({4-[(furan-2-yl)methyl]-5-(1*H*-indol-3-yl)-4*H*-1,2,4-triazol-3-yl)sulfonyl}acetamid (NCE2).

A vial was charged with 4-Furan-2-ylmethyl-5-indol-3-ylidene-[\[1,2,4\]](#)triazolidene-3-thione (1.0 equiv.), DMF (2 ml), DIPEA (1.2 equiv.). To the stirred mixture 2-Chloro-*N*-(2-chloro-benzyl)-acetamide (1.0 equiv.) was added. The vial was capped and heated while stirring for 1 hr. After 30 min, the reaction mixture became clear and heating was continued for further 3 hrs. Then the vial was cooled, diluted with water, and the precipitate formed was filtered off, washed with water and dried. The average yield was 20%; mp, 184–185 °C; 1H NMR (400 MHz, DMSO- D_6), δ 4.03 (s, 2H, $-CH_2-S$), 4.35–4.36 (d, 2H, $^3J = 5.54$ Hz, $-CH_2-NH$), 5.39 (s, 2H, $-CH_2-N$ -triazole), 6.39–6.44 (m, 2H, H-furan), 7.12–7.16 (m, 1H, aromatic), 7.19–7.27 (m, 3H, aromatic), 7.33–7.35 (m, 1H, aromatic), 7.38–7.41 (m, 1H, aromatic), 7.49–7.51 (d, 1H, $^3J = 8.18$ Hz, aromatic), 7.63–7.64 (m, 1H, aromatic), 7.91 (s, 1H, indole C-H), 8.05–8.07 (d, 1H, $^3J = 7.90$ Hz, aromatic), 8.81–8.84 (t, 1H, $^3J = 6.14$ Hz, NH -amide), 11.76 (s, 1H, NH -indole); ^{13}C NMR (100 MHz, DMSO- D_6), δ 37.4, 79.6, 101.6, 109.6, 111.2, 112.3, 120.7, 121.3, 122.9, 125.9, 126.2, 127.6, 129.1, 129.3, 129.5, 132.4, 136.3, 136.4, 144.0, 148.9, 149.5, 151.9, 167.8; MS (APCI): $m/z = 478$ [$M^+ + H$].

4.1.4. *N*-(4-ethylphenyl)-5-(2-hydroxy-5-methoxybenzoyl)-2-imino-2*H*-pyran-3-carboxamide (NCE3).

The reaction was carried out in 8 ml glass vial. The reactants were loaded in view that 1.0 equivalent is equal to 0.75 mmol of the compound. A vial was charged with 6-Methoxy-4-oxo-4*H*-chromene-3-carbaldehyde (1.0 equiv.) and corresponding 2-Cyano-*N*-(4-ethyl-phenyl)-acetamide active compound (1.0 equiv.), acetic acid (5 ml), and sodium acetate (1.1 equiv.). The vial was capped and heated at 100 °C for 8 hrs. Then it was cooled and diluted with water (5 ml). The formed precipitate was filtered, dried, and re-crystallized from acetonitrile. The yield was 48%; mp, 132–133 °C; 1H NMR (400 MHz, $CDCl_3$), δ 1.25–1.29 (t, 3H, $^3J = 7.68$ Hz, $-CH_3$), 2.69–2.74 (q, 2H, $^3J = 7.68$ Hz, $-CH_2$), 3.77 (s, 3H, $-OCH_3$), 6.95–6.69 (d, 1H, $^4J = 2.94$ Hz, aromatic), 7.02–7.04 (d, 1H, $^3J = 9.00$ Hz, aromatic), 7.15–7.18 (dd, 1H, $^3J = 9.14$ Hz and $^4J = 3.09$ Hz, aromatic), 7.27–7.30 (m, 2H, aromatic), 7.34–7.37 (m, 2H, aromatic), 8.22–8.23 (d, 1H, $^4J = 2.65$ Hz, C-H pyrimidine), 8.30–8.31 (d, 1H, $^4J = 2.65$ Hz, C-H pyrimidine), 10.67 (s, 1H, NH -amide); ^{13}C NMR (100 MHz, $CDCl_3$), δ 15.3, 28.5, 55.9, 106.0, 114.0, 114.4, 116.6, 117.8, 120.0, 124.3, 125.7, 129.3, 136.4, 146.6, 146.8, 147.3, 151.9, 156.7, 158.6, 192.7; MS (APCI): $m/z = 395$ [$M^+ + H$].

4.1.5. 2-(4-sulfamoylphenoxy)ethyl 2-amino-3-methylbenzoate (NCE 4).

The reaction was carried out in 8 ml glass vial. The reactants were loaded in view that 1.0 equivalent is equal to 1.4 mmol of the compound. A vial was charged with 2-Amino-3-methyl-benzoic acid (1.2 equiv.), DMF (2 ml), and DIPEA (1.2 equiv.). To the stirred mixture in the vial, 4-(2-Bromo-ethoxy)-benzenesulfonamide (1.0 equiv.) was added. The vial was capped and heated under stirring for 1 hr. After 30 min the reaction mixture became clear and heating was continued for further 6 hrs at 100 °C. Then the vial was cooled, diluted with water, and extracted with chloroform. The combined organic layers were dried over concentrated sodium sulfate. The crude product was purified with CombiFlash chromatography on silica gel. The average yield was 50%; mp, 165–166 °C; 1H NMR (400 MHz, DMSO- D_6), δ 2.10 (s, 3H, $-CH_3$), 4.39–4.41 (t, 2H, $^3J = 7.60$ Hz, $-CH_2$), 4.54–4.56 (t, 2H, $^3J = 7.60$ Hz, $-CH_2$), 6.46–6.49 (m, 2H, aromatic CH and NH_2), 7.14–7.19 (m, 3H, aromatic), 7.24 (s, 2H, Ar- NH_2), 7.59–7.61 (dd, 1H, $^3J = 8.13$ Hz and $^4J = 1.05$ Hz, aromatic), 7.73–7.75 (m, 2H, aromatic); ^{13}C NMR (100 MHz, DMSO- D_6), δ 18.1, 62.8, 66.8, 108.8, 115.1, 123.8, 128.2, 129.0, 135.4, 136.9, 150.1, 161.1, 168.2; MS (APCI): $m/z = 351$ [$M^+ + H$].

4.1.6. *N*-(3-([carbamoyl(phenyl)methyl]amino)phenyl)-2-methoxypropanamide (NCE5).

The reaction was carried out in 8 ml glass vial. The reactants were loaded in view that 1.0 equivalent is equal to 1.8 mmol of the compound. To a stirred solution containing specified amounts of *m*-aminophenyl-2-methoxypropanamide (1.0 equiv.), DIPEA (1.1 equiv.), and potassium iodide (catalyst) in 1 ml of DMF and benzylchloridmethanamide (1.0 equiv.) was added. The reaction mixture was allowed to stir on a boiling water bath for 5 min. Upon complete dissolution of the reagents the stirred reaction mixture was heated on the water bath for further 6 hrs. The reaction mixture was saturated with an excess of deionized water and sonicated until a crystalline precipitate was formed. The precipitate was filtered, washed twice with methanol, and dried. The crude product was purified by chromatography (silica gel, $CHCl_3$:iPrOH = 4:1). The yield was 30%; mp, 167–168 °C; 1H NMR (400 MHz, DMSO- D_6), δ 1.26–1.27 (d, 3H, $^3J = 6.63$ Hz, $-CH_3$), 3.26 (s, 3H, $-CH_3$), 3.79–3.84 (q, 1H, $^3J = 6.81$ Hz, $-CH$), 4.88–4.89 (d, 1H, $^3J = 5.29$ Hz, $-CH$), 6.06–6.07 (d, 1H, $^3J = 7.19$ Hz, aromatic), 6.36–6.38 (d, 1H, $^3J = 7.19$ Hz, aromatic), 6.82–6.84 (m, 1H, aromatic), 6.92–6.97 (m, 1H, aromatic), 7.06 (s, 1H, $-NH_2$), 7.20 (s, 1H, $-NH_2$), 7.23–7.27 (m, 1H, aromatic), 7.31–7.35 (m, 2H, aromatic), 7.49–7.52 (m, 2H, aromatic), 7.71 (s, 1H, amide N-H), 9.51–9.53 (d, 1H, $^3J = 5.11$ Hz, amide N-H); ^{13}C NMR (100 MHz, DMSO- D_6), δ 18.8,

57.1, 60.8, 79.6, 104.9, 105.0, 108.9, 109.4, 127.7, 127.9, 128.7, 129.2, 139.6, 140.2, 147.9, 171.3, 173.1 MS (APCI): m/z = 328 [M^+ + H].

4.1.7. 1-(4-butanamidophenyl)-1-oxopropan-2-yl-1H-indazole-3-carboxylate (NCE6)

The reaction was carried out in 8 ml glass vial. The reactants were loaded in view that 1.0 equivalent is equal to 1.4 mmol of the compound. A vial was charged with 1H-Indazole-3-carboxylic acid (1.2 equiv.), DMF (2 ml), and DIPEA (1.2 equiv.). To the stirred mixture N-[4-(2-Chloro-propionyl)-phenyl]-butyramide (1.0 equiv.) was added. The vial was capped and heated under stirring for an 1hr. After 30 min, the reaction mixture became clear and heating was continued for the next 6hrs at 100 °C. Then the vial was cooled, diluted with water, and extracted with chloroform. The combined organic layers were dried over concentrated sodium sulfate. The crude product was purified with CombiFlash chromatography on silica gel. The average yield was 50%; mp, 205–206 °C; ^1H NMR (400 MHz, DMSO- D_6) δ 0.91–0.94 (t, 3H, 3J = 7.36 Hz, $-\text{CH}_3$), 1.63–1.67 (m, 5H, $-\text{CH}_2$ and $-\text{CH}_3$), 2.32–2.36 (t, 2H, 3J = 7.46 Hz, $-\text{CH}_2$), 6.31–6.41 (q, 1H, 3J = 6.86 Hz, $-\text{CH}$), 7.32–7.36 (m, 1H, aromatic), 7.46–7.50 (m, 1H, aromatic), 7.69–7.71 (d, 1H, 3J = 8.23 Hz, aromatic), 7.79–7.81 (d, 2H, 3J = 8.85 Hz, aromatic), 8.05–8.09 (m, 3H, aromatic), 10.31 (s, 1H, $-\text{NH}$), 14.04 (s, 1H, $-\text{COOH}$); ^{13}C NMR (100 MHz, DMSO- D_6) δ 14.1, 17.8, 18.9, 72.1, 111.7, 118.9, 121.4, 122.7, 123.5, 127.2, 128.6, 130.3, 135.0, 141.4, 144.8, 161.9, 172.4, 195.5; MS (APCI): m/z = 380 [M^+ + H].

4.1.8. N-(2-hydroxyphenyl)-4-{3-[(2-hydroxyphenyl)carbamoyl]phenoxy}benzamide (NCE7)

NCE 7 was synthesized by using the general procedure in method C; mp, 266–267 °C; ^1H NMR (400 MHz, DMSO- d_6) δ 6.81–6.85 (m, 2H, aromatic), 6.91–6.93 (dd, 2H, 3J = 8.06 Hz and 4J = 1.27 Hz aromatic), 7.01–7.06 (m, 2H, aromatic), 7.20–7.22 (m, 4H, aromatic), 7.64–7.66 (dd, 2H, 3J = 8.06 Hz and 4J = 1.27 Hz, aromatic), 8.04–8.07 (m, 4H, aromatic) Hz δ 9.56 (s, 2H, $-\text{NH}$ -amide); ^{13}C NMR (100 MHz, DMSO- D_6) δ 116.5, 119.1, 119.4, 124.8, 126.2, 126.3, 130.3, 130.4, 150.0, 159.2, 164.9; MS (APCI): m/z = 340 [M^+ + H].

4.1.9. 2-chloro-N-(3-[(6-chloro-3-oxo-3,4-dihydro-2H-1,4-benzoxazin-7-yl)amino]methyl)phenyl)benzamide (NCE8)

NCE 8 was synthesized by using the general procedure for method B; mp, 231–232 °C; ^1H NMR (400 MHz, DMSO- D_6) δ 4.36 (s, 2H, $-\text{CH}_2\text{-N}$ and 2'), 4.42 (s, 2H, $-\text{CH}_2\text{-O}$), 4.45 (s, 1H, 2' amine N-H) 6.14 (s, 1H, aromatic), 6.82 (s, 1H, aromatic), 7.08–7.09 (m, 1H, aromatic), 7.27–7.31 (m, 1H, aromatic), 7.42–7.74 (m, 6H, aromatic), 10.41 (s, 1H, amide N-H), 10.50 (s, 1H, amide N-H); ^{13}C NMR (100 MHz, DMSO- D_6) δ 67.3, 79.7, 100.5, 103.6, 110.6, 111.1, 116.5, 122.7, 127.9, 129.3, 129.4, 130.1, 130.6, 131.5, 137.6, 139.8, 140.7, 141.2, 143.8, 164.2, 165.4; MS (APCI): m/z = 443 [M^+ + H].

4.1.10. 3-[(6-hydroxy-3-oxo-3,4-dihydro-2H-1,4-benzoxazin-7-yl)amino]methyl-N-(pyridin-3-yl)benzamide (NCE8a)

NCE 8a was synthesized by using the general procedure for method A; mp, 231–232 °C; ^1H NMR (400 MHz, DMSO- D_6) δ 4.39 (s, 2H, $-\text{CH}_2\text{-N}$), 4.45 (s, 2H, $-\text{CH}_2\text{-O}$), 4.50 (s, 1H, 2' amine N-H), 6.54 (s, 2H, aromatic), 7.55–7.59 (m, 1H, aromatic), 7.65–7.67 (m, 1H, aromatic), 7.94–8.11 (m, 3H, aromatic), 8.56–8.64 (m, 2H, aromatic), 9.34–9.35 (d, 1H, 4J = 2.08 Hz, pyridine-H), 10.56 (s, 1H, amide N-H), 11.23 (s, 1H, amide N-H); MS (APCI): m/z = 391 [M^+ + H].

4.1.11. 3-[(3-oxo-3,4-dihydro-2H-1,4-benzoxazin-7-yl)amino]methyl-N-(pyridin-3-yl)benzamide (NCE 8b)

NCE 8b was synthesized by using the general procedure for method A; mp, 118–119 °C; ^1H NMR (400 MHz, DMSO- D_6) δ 4.29–4.30 (d, 2H, 3J = 5.45 Hz, $-\text{CH}_2\text{-NH}$), 4.41 (s, 2H, $-\text{CH}_2\text{-O}$), 6.17–6.25 (m, 2H, aromatic), 6.59–6.13 (d, 1H, 3J = 8.33 Hz, aromatic), 7.34–7.41 (m,

1H, aromatic), 7.47–7.51 (m, 1H, aromatic), 7.56–7.58 (1H, d, 3J = 7.78 Hz, aromatic), 7.83–7.85 (d, 1H, 3J = 7.63 Hz, aromatic), 7.94 (s, 1H, aromatic), 8.17–8.19 (m, 1H, pyridine-H), 8.30–8.32 (m, 1H, aromatic), 8.92 (d, 1H, 4J = 2.31 Hz, pyridine-H), 10.31 (s, 1H, amide N-H), 10.47 (s, 1H, amide N-H); ^{13}C NMR (100 MHz, DMSO- D_6) δ 67.2, 79.6, 100.7, 106.8, 116.7, 123.7, 126.9, 127.0, 127.7, 128.8, 130.9, 134.8, 136.2, 141.3, 142.4, 144.6, 144.9, 145.5, 164.3, 166.3; MS (APCI): m/z = 375 [M^+ + H].

4.1.12. N-(2-hydroxyphenyl)-3-[(3-oxo-3,4-dihydro-2H-1,4-benzoxazin-7-yl)amino]methylbenzamide (NCE 8c)

NCE 8c was synthesized by using the general procedure of method A; 192–193 °C; ^1H NMR (400 MHz, DMSO- D_6) δ 4.28–4.29 (d, 2H, 3J = 5.67 Hz, $-\text{CH}_2\text{-NH}$), 4.40 (s, 2H, $-\text{CH}_2\text{-O}$), 6.18–6.27 (m, 2H, aromatic), 6.59–6.61 (d, 1H, 3J = 8.36 Hz, aromatic), 6.73–6.82 (m, 1H, aromatic), 6.89–6.92 (dd, 1H, 3J = 7.99 Hz and 4J = 1.23 Hz, aromatic), 7.04–7.09 (m, 1H, aromatic), 7.44–7.48 (m, 1H, aromatic), 7.53–7.55 (d, 1H, 3J = 7.60 Hz, aromatic), 7.67–7.69 (d, 1H, 3J = 7.78 Hz, aromatic), 7.81–7.82 (d, 1H, 3J = 7.60 Hz, aromatic), 9.49 (s, 1H, amide N-H), 10.29 (s, 1H, amide N-H); ^{13}C NMR (100 MHz, DMSO- D_6) δ 67.3, 79.8, 100.8, 106.9, 116.4, 116.8, 117.2, 119.4, 126.1, 126.3, 126.8, 128.9, 130.9, 134.9, 141.4, 144.7, 145.6, 164.3, 165.7; MS (APCI): m/z = 390 [M^+ + H].

4.1.13. N-(4-chloro-3-[(3-oxo-3,4-dihydro-2H-1,4-benzoxazin-7-yl)carbamoyl]phenyl)-1H-pyrazole-4-carboxamide (NCE8d)

NCE 8d was synthesized by using the general procedure for method B; mp, 308–309 °C; ^1H NMR (400 MHz, DMSO- d_6) δ 4.56 (s, 2H, $-\text{CH}_2\text{-O}$), 6.85–6.87 (d, 1H, 3J = 8.48 Hz, aromatic), 7.26–7.29 (dd, 1H, 3J = 8.01 Hz and 4J = 2.18 Hz, aromatic), 7.39–7.40 (d, 1H, 4J = 2.18 Hz, aromatic), 7.50–7.52 (d, 1H, 3J = 8.75 Hz, aromatic), 7.86–7.89 (m, 2H, aromatic), 8.07 (s, 1H, pyrazole-H), 8.38 (s, 1H, pyrazole-H), 10.06 (s, 1H, amide N-H), 10.49 (s, 1H, amide N-H), 10.69 (s, 1H, amide N-H), 10.33 (s, 1H, pyrazole N-H); ^{13}C NMR (100 MHz, DMSO- D_6) δ 62.3, 108.3, 114.0, 116.2, 118.0, 120.0, 122.3, 123.7, 123.8, 130.4, 134.7, 137.3, 138.8, 143.6, 161.1, 164.9, 165.0; MS (APCI): m/z = 412 [M^+ + H].

4.1.14. 3-[(6-chloro-3-oxo-3,4-dihydro-2H-1,4-benzoxazin-7-yl)amino]methyl-N-(pyridin-3-yl)benzamide (NCE8e)

NCE 8e was synthesized by using the general procedure for method A; mp, 230–231 °C; ^1H NMR (400 MHz, DMSO- D_6) δ 4.42 (s, 2H, $-\text{CH}_2\text{-N}$), 4.44 (s, 2H, $-\text{CH}_2\text{-O}$), 6.13 (s, 1H, aromatic), 6.79 (s, 1H, aromatic), 7.38–7.41 (dd, 1H, 3J = 7.89 Hz and 3J = 4.68 Hz, aromatic), 7.48–7.56 (m, 2H, aromatic), 7.83–7.84 (d, 1H, 3J = 7.69 Hz, aromatic), 7.92 (s, 1H, aromatic), 8.16–8.19 (m, 1H, aromatic), 8.30–8.31 (dd, 1H, 3J = 4.68 Hz and 4J = 1.43 Hz, pyridine-H), 8.90–8.91 (d, 1H, 4J = 2.17 Hz, pyridine-H), 10.41 (s, 1H, amide N-H), 10.48 (s, 1H, amide N-H); ^{13}C NMR (100 MHz, DMSO- D_6) δ 67.2, 79.6, 100.5, 111.0, 124.0, 126.5, 126.9, 127.8, 128.9, 135.0, 136.2, 140.4, 140.9, 142.4, 143.6, 145.0, 164.2, 166.5; MS (APCI): m/z = 409 [M^+ + H].

4.2. Computational data

Table 1 shows the 78 studied inhibitors. They have ten different core structures (Class) and exhibit broad inhibition activity to CYP17A1 enzyme (*in vitro* experimental IC_{50} between 13 and 20000 nM collected from the literature [2,9,13,19,28,42–43]). The IC_{50} values in molar units were converted into pIC_{50} data for 3D-QSAR partial least squares (PLS) modeling purposes. The inhibitors (in decreasing order of pIC_{50}) are named as in the original references. They were randomly divided into 63 training (subset 1) and 15 test (subset 2) compounds for model validation.

4.2.1. Computational software program

Maestro (v10.2) [58], a graphical user interface (GUI) in

Schrödinger Suite 2015, was used to perform all simulation tasks. The GUI has built-in workflows for all Schrödinger modules in the suite. Conformational searches were performed by using MacroModel (v10.8) [59]. Pharmacophore modeling was performed by using PHASE (v4.3) [60–62], a module of the Schrödinger suite. A virtual Screening Workflow, VSW [63], was employed on the database hit compounds. Quantum mechanical/molecular mechanics calculations (Density functional theory, DFT) were done by using Jaguar (v8.8) [64]. Cross-docking was used to validate docking methods. Cross-docking was performed by using the Glide cross-docking script with default parameters. Compounds that survived the virtual screening procedure were subjected to Induced Fit Docking (IFD) [65]. IFD was used for all flexible molecular docking calculations of database hits screened.

4.2.2. Preparation of structures

The inhibitors were introduced into the PHASE software as 2D structures and converted into 3D formats. Tautomers were generated for low-energy structures at pH 7.4 and every combination of stereoisomers was generated (Ligprep module). The 3D structures were then subjected to a conformational search (MacroModel). OPLS-2005 force-field was used to generate low-energy multiple conformers with a constant dielectric constant of 1.0. The number of minimization steps was set to 100. An energy change of 10 kcal/mol was set for saving multiple conformers. A root-mean-square-deviation (RMSD) cut-off of 1.0 Å was set to eliminate unnecessary conformers.

4.2.3. Pharmacophore modeling

The resulting conformers were mapped against fixed chemical features. The pharmacophore features included hydrogen bond acceptors (A), hydrogen bond donors (D), negatively charged groups (N), positively charged groups (P), hydrophobic groups (H) and aromatic rings (R). The development of the pharmacophore model was performed according to previously reported information [45,46]. Briefly, the search spanned different families of pharmacophores. The number of site points on the data set was six, taken from the 12 most active inhibitors in the training set (Table 1; $IC_{50} < 40$ nM). The best common pharmacophore hypothesis (CPH) was selected as the one showing the 3D-QSAR PLS model with the best prediction ability (i.e. the one showing the highest determination coefficient for the training and test compounds, R^2 and Q^2 respectively). The conformer with the highest fitness score (matching degree between the molecule and the best CPH) was selected as reference compound.

4.2.4. Preparation of a 3D database and pharmacophore screening

A structural database was prepared prior to using the 3D-QSAR model for database screening. 2.5 million drug-like structures were downloaded from the Enamine LTD database [66] and added into the Manage 3D Database panel in PHASE module. The 3D database was prepared by generating ionization states for structures using the PHASE submodule Epik at pH 7.4. Structures with high ionization energy and/or high tautomerization states were removed. Structures with undesirable functional groups (from a toxicity point of view) were removed. Furthermore, structures that did not satisfy Lipinski's rule of five were also removed. The 3D-QSAR pharmacophore model was used for database screening. The most active hits (estimated $pIC_{50} > 7$) having the 6 pharmacophore sites of the best CPH were selected for further studies.

4.2.5. Virtual screening Workflow

A virtual screening workflow, with built in GlideSP and GlideXP was used to screen drug-like molecules from the database. Virtual Screening Workflow provided a reduced number of hit structures after they were screened. Selected hits were submitted to geometry optimization using DFT and further molecular docking using IFD. In the VSW ligand preparation was deselected as the ligands were already prepared during Phase database screening. The remaining ligands were docked on the

prepared and minimized structure of 3SWZ grid. Glide SP and Glide XP (both built into VSW) were consecutively used. Hits that survived Glide SP were further docked with Glide XP.

4.2.6. Density functional theory calculations

A geometry optimization calculation using a DFT procedure and a basis set function of B3LYP 6-31G* in the Jaguar panel [47,48,64] was used to calculate the electronic properties of the hits. It was then followed by a single-point energy calculation at the optimum geometries to obtain aqueous solution phase energies using a continuum treatment of solvation by Poisson-Boltzmann modeling [48]. The electronic properties of interest calculated included the following: molecular electrostatic potential (MESP), highest occupied and lowest unoccupied molecular orbital (HOMO and LUMO, respectively), and electron density map [47].

4.2.7. Cross-docking

Cross-docking was employed to select the suitable PDB structure and to validate the IFD protocol. In cross-docking the co-crystallized ligand of the receptor is removed and then subsequently re-docked into the receptor using Glide/cross-docking script. The main idea is to reproduce the binding mode of the x-ray crystal structure of the protein-ligand complex. The 3SWZ and 3RUK PDB X-ray structures, with co-crystallized structures of galeterone and abiraterone, respectively, were tested. The comparison of results from IFD and cross-docking allowed the selection of the PDB enzyme structure for subsequent studies, based on the following criteria: (i) resolution of the enzyme x-ray crystal structure (ii) docking score, (iii) Root Mean Square Deviation (RMSD). Indirectly, the agreement between the outputs served as a validation of the IFD protocol.

4.2.8. Flexible ligand docking with Induced fit Docking.

A flexible ligand-protein molecular docking procedure was performed using the Glide/IFD protocols [49], since the charges for a free ligand have been previously calculated by a hybrid quantum mechanical calculation (DFT optimization). In this docking protocol, the conformational change of the enzyme and the ligand during binding are accounted for. Since CYP17A1 is a flexible enzyme, it was important to yield conformers close to the real *in vivo* conformation. The drug-like molecules that survived VSW were incorporated into Glide/IFD. The 3SWZ structure (already prepared and minimized) was added. The co-crystallized ligand in the active site cavity of the enzyme was frozen and used to mark the active site of the enzyme; that new compounds need to occupy. Several rules were fixed as filtering criteria for screening hits obtained by IFD: (i) the binding mode of the selected pose should correspond preferably to type I inhibition; since it has been related to a selective lyase inhibition [25]. However, the presence of a metal coordination with ferric heme (type II inhibition) is also allowed; (ii) the ligand pose should possess metal binding groups such as N-containing heterocycles e.g. pyridine rings [19], because N-containing heterocycles form π - π interactions with porphyrin of ferric heme; (iii) a docking score < -6 kcal/mol; (iv) and the presence of a hydrogen bond with ASN202 [23,25]. The hits that satisfied the four criteria were retained.

4.3. Inhibition of NCEs on the hydroxylase and lyase activities of human CYP17A1 expressed in *E. coli* bactosomes

The compounds synthesized in Section 5.2. above were used for the inhibition of the hydroxylase and lyase activities. The method to estimate IC_{50} values was adapted from [13].

4.3.1. Reagents

Imipramine, abiraterone and pregnenolone were purchased from Santa Cruz Biotechnologies (Heidelberg, Germany), dehydroepiandrosterone (DHEA), magnesium chloride, DMSO and phosphate buffer

were purchased from Sigma-Aldrich (Gillingham, UK), ketoconazole was purchased from Sequoia Research Products Ltd. (Pangbourne, UK) and 17 α -hydroxypregnenolone was purchased from Carbosynth (Compton, UK). Co-factors such as nicotinamide adenine dinucleotide phosphate (NADPH), CYP17A1-LR bacosomes and CYP17A1-BR bacosomes were purchased from Cypex (Dundee, UK). HPLC-MS-grade methanol and formic acid were from Fisher Scientific (Loughborough, UK). Water was purified on a Milli Q system (Millipore, Watford, UK).

4.3.2. CYP17A1 hydroxylase and lyase incubations

The CYP17A1 17 α -hydroxylase and lyase inhibition was measured using bacosomes solution. 20 pmol/ml CYP17A1-LR and 10 pmol/ml CYP17A1-BR bacosomes were used for hydroxylase and lyase assays, respectively. Pregnenolone and 17 α -hydroxypregnenolone were used as substrates for hydroxylase and lyase assays, respectively. 1 μ M substrate solution prepared by dilution of the stock solution 10 μ M of pregnenolone and 17 α -hydroxypregnenolone. 1 mM NADPH was prepared in 50 mM potassium phosphate buffer pH 7.4 containing 5 mM magnesium chloride. Stock solutions of 16 mM of the synthesized NCEs in DMSO were prepared. In addition, stock solution of 10 mM of ABT as a positive control inhibitor in DMSO was prepared. NCEs and the positive control inhibitor were diluted serially (2.5-fold) in eight steps yielding final assay concentrations of 160 μ M – 0.26 μ M (NCEs) and 500 nM to 0.82 nM (positive control inhibitor). Reactions were started by the addition of NADPH and incubated at 37 °C for 20 min with shaking on a Bioshake IQ (Q-Instruments, Jena, Germany). Reaction volume was 100 μ L and final DMSO concentration was 1% (v/v). Reactions were terminated by the addition of 300 μ L of methanol containing 25 ng/mL imipramine as an internal standard (IS). The enzyme activity was assessed by measuring the appearance of the corresponding metabolite using UHPLC-MS/MS. Finally, 17 α -hydroxypregnenolone and DHEA were the metabolites obtained, for hydroxylase and lyase assays, respectively. The experiments were performed by means of ultra high performance liquid chromatography-tandem mass spectrometry (UHPLC-MS/MS). All the assays were performed in duplicates.

4.3.3. UHPLC-MS/MS analysis

A Vanquish UHPLC system (ThermoFisher Scientific, Runcorn, UK) with a binary pump and an autosampler was used. The mobile phase flow rate was 0.8 ml/min and the column temperature was set at 60 °C. The injection volume was 3.5 μ L. The separation was performed using an Accucore, (C18, 2.6 μ m, 50 \times 2.1 mm, Runcorn, UK) column. The following gradient elution was carried out using different ratios of eluents A (0.1% formic acid in water) and B (0.1% formic acid in methanol): 0–0.69 min, 5% B; 0.70–1.14 min, 95% B; 1.15 min, 99.9% B; 1.16–1.40 min, 5% B for column re-equilibration.

A triple quadrupole mass spectrometer (TSQ Quantiva, Thermo Fisher Scientific) with multiple reaction monitoring (MRM) was used for MS detection. The instrument was operated using atmospheric pressure chemical ionisation (APCI) in positive mode. Nitrogen was used as auxiliary and sheath gas, and argon was used as collision gas. The following ion source conditions were used: vaporizer temperature, 500 °C; ion transfer tube temperature, 275 °C; positive ion discharge current, 1 μ A; sheath gas, 45 AU; auxiliary gas, 5 AU; sweep gas, 2 AU. The MS/MS parameters were the following: collision gas pressure, 1.5 mTorr; source fragmentation voltage, 0 V; chrom filter, 2 s; and dwell time, 10 ms. The MRM transitions, collision energies and RF lens of the analytes and IS are shown in Table 4. Xcalibur software (v4.0) was used for data analysis.

4.3.4. Data analysis

Each sample was analysed for the analyte (DHEA or 17-OH-Pregnenolone) and the IS, yielding a peak area for the analyte (A_{analyte}) and one for the IS (A_{IS}). MS response (R) was calculated by dividing A_{analyte} by A_{IS} .

Table 4

Multiple reaction monitoring (MRM) transitions, RF lens and collision energies for LC-MS/MS measurements.

Compound	Precursor (m/z)	Product (m/z)	RF Lens (V)	Collision energy (V)
17 α -Hydroxypregnenolone	315.23	201.10	49	17
		279.15	49	14
		297.17	49	10
Dehydroepiandrosterone (DHEA)	271.23	197.11	51	17
		213.10	51	15
		253.15	51	12
Imipramine (internal standard)	281.13	86.11	50	16
		193.00	50	41
		208.00	50	26

Note: Mass transitions for each compound were combined to maximize sensitivity.

$$R = \frac{A_{\text{analyte}}}{A_{\text{IS}}} \quad (1)$$

The activity remaining (%) in the presence of an inhibitor was calculated as the ratio of response in the presence of the inhibitor ($R_{\text{inhibitor}}$) divided by the response in the absence of inhibitor (R_{control}) multiplied by 100%.

$$\text{Activity remaining (\%)} = \frac{R_{\text{inhibitor}}}{R_{\text{control}}} \quad (2)$$

The activity remaining is the same as the effect E in the Hill equation presented below. In the hydroxylase activity calculation DHEA detected is not counted. Since the % abundance of the DHEA signal is less than 5% (see Table S4). The IC_{50} values were estimated by fitting the concentration-effect curve data of the inhibitors to a modified version of the Hill equation [67,68].

$$E = \frac{\alpha [I]^{nH}}{[I]^{nH} + IC_{50}^{nH}} \quad (3)$$

where E is expressed in percentage, α is the upper asymptotes (maximum effect), [I] is the inhibitor concentration and nH is the Hill slope.

Author contributions

The authors contributed equally. All authors have given approval to the final version of the manuscript.

Declaration of Competing Interest

NJG is the registered inventor on the two patents that are pending in national and regional phases: (PCT/ZA2016/050041 and PCT/ZA2016/050042). The authors wish to confirm that there are no known conflicts of interest associated with this publication, and there has been no significant financial support for this work that could have influenced its outcome.

Acknowledgments

This work research work was supported financially in part by the National Research Foundation of South Africa and First Rand Foundation (UID: 112151). This work was also made possible through funding by the Research Capacity Development Initiative-South African Medical Research Council (RCDI-SAMRC). The content hereof is the sole responsibility of the authors and does not necessarily represent the official views of NRF and SAMRC. The authors would like to acknowledge the Centre for High Performance Computing for allowing access to their resources for molecular modeling. Xenogenesis Ltd is greatly acknowledged for performing bioanalytical experiments, as an

outsourced services. Enamine LTD is greatly acknowledge for custom synthesis of the compounds, as an outsourced service.

Appendix A. Supplementary material

Supplementary data to this article can be found online at <https://doi.org/10.1016/j.bioorg.2019.103462>.

References

- I.P. Nnane, K. Kato, Y. Liu, B.J. Long, Q. Lu, X. Wang, Y.Z. Ling, A. Brodie, Inhibition of androgen synthesis in human testicular and prostatic microsomes and in male rats by novel steroidal compounds, *Endocrinology* 140 (1999) 2891–2897.
- C. Jagusch, M. Negri, U.E. Hille, Q. Hu, M. Bartels, K. Jahn-Hoffmann, M.A.E. Pinto-Bazurco Mendieta, B. Rodenwaldt, U. Müller-Vieira, D. Schmidt, T. Lauterbach, M. Recanatini, A. Cavalli, R.W. Hartmann, Synthesis, biological evaluation and molecular modelling studies of methylene imidazole substituted biaryls as inhibitors of human 17 α -hydroxylase-17,20-lyase (CYP17). Part I: Heterocyclic modifications of the core structure, *Bioorg. Med. Chem. J.* 16 (2008) 1992–2010.
- S.M. Haider, J.S. Patel, C.S. Poojari, S. Neidle, Molecular Modeling on inhibitor complexes and active-site Dynamics of Cytochrome P450 C17, a target for prostate cancer therapy, *J. Mol. Biol.* 400 (2010) 1078–1098.
- T.A. Yap, C.P. Carden, G. Attard, J.S. de Bono, Targeting CYP17: established and novel approaches in prostate cancer, *Curr. Opin. Pharmacol.* 8 (2008) 449–457.
- E. Gianti, R.J. Zauhar, Modeling androgen receptor flexibility: a binding mode hypothesis of CYP17 inhibitors/antiandrogens for prostate cancer therapy, *J. Chem. Inf. Model.* 52 (2012) 2670–2683.
- G. Schaefer, J.M. Mosquera, R. Ramoner, K. Park, A. Romanel, E. Steiner, W. Horninger, J. Bektic, M. Ladurner-Rennau, M.A. Rubin, F. Demichelis, H. Klocker, Distinct ERG rearrangement prevalence in prostate cancer: higher frequency in young age and in low PSA prostate cancer, *Prostate Cancer P. D.* 16 (2013) 132–138.
- G. Lippolis, A. Edsjö, U.H. Stenman, A. Bjartell, A high density tissue micro-array from patients with clinically localized prostate cancer reveals ERG and TATI exclusivity in tumor cells, *Cancer P. D.* 16 (2013) 145–150.
- R. Ferraldeschi, J. de Bono, Agents that target androgen synthesis in castration-resistant prostate cancer, *Cancer J.* 19 (2013) 34–42.
- Q. Hu, C. Jagusch, U.E. Hille, J. Hauptenthal, R.W. Hartmann, Replacement of imidazolyl by pyridyl in biphenylmethylenes results in selective CYP17 and dual CYP17/CYP11B1 inhibitors for the treatment of prostate cancer, *J. Med. Chem.* 53 (2010) 5749–5758.
- A.E. Mariano, P. Mendieta, Q. Hu, M. Engel, R.W. Hartmann, Highly potent and selective nonsteroidal dual inhibitors of CYP17/ CYP11B2 for the treatment of prostate cancer to reduce risks of cardiovascular diseases, *J. Med. Chem.* 56 (2013) 6101–6107.
- T. Kaku, S. Tsujimoto, N. Matsunaga, T. Tanaka, T. Hara, M. Yamaoka, M. Kusaka, A. Tasaka, 17,20-Lyase inhibitors. Part 3: Design, synthesis, and structure-activity relationships of biphenylmethylimidazole derivatives as novel 17, 20-lyase inhibitors, *Bioorg. Med. Chem.* 19 (2011) 2428–2442.
- R.D. Bruno, T.S. Vasaitis, L.K. Gediya, P. Purushottamachar, A.M. Godbole, Z. Ates-Alagoz, A.M.H. Brodie, V.C.O. Njar, Synthesis and biological evaluations of putative metabolically stable analogs of VN/124-1 (TOK-001): Head to head anti-tumor efficacy evaluation of VN/124-1 (TOK-001) and abiraterone in LAPC-4 human prostate cancer xenograft model, *Steroids* 76 (2011) 1268–1279.
- S.J. Krug, Q. Hu, R.W. Hartmann, Hits identified in library screening demonstrate selective CYP17A1 lyase inhibition, *J. Ster. Biochem. Mol. Biol.* 134 (2013) 75–79.
- J.D. McConnel, H.B. Carter, Physiologic basis of endocrine therapy for prostatic cancer, *Urol. Clin. North Am.* 18 (1991) 1–13.
- W.L. Miller, Molecular Biology of steroid hormone synthesis, *Endocr. Rev.* 9 (1990) 295–318.
- D.F. Easton, D.J. Schaid, A.S. Whitmore, W.J. Isaacs, where are the prostate cancer genes? A summary of eight genome wide searches, *Prostate* 57 (2003) 261–269.
- H. Zhu, J.A. Garcia, Targeting the adrenal gland in castration-resistant prostate cancer: a case for orteronel, a selective CYP-17 17,20-Lyase Inhibitor, *Curr. Oncol. Rep.* 15 (2013) 105–112.
- M. Wang, Y. Fang, S. Gu, F. Chen, Z. Zhu, X. Sun, J. Zhu, Discovery of novel 1,2,3,4-tetrahydrobenzo[4, 5]thieno[2, 3-c]pyridine derivatives as potent and selective CYP17 inhibitors, *Eur. J. Med. Chem.* 132 (2017) 157–172.
- S.W. Rafferty, J.R. Eisner, W.R. Moore, R.J. Schotzinger, W.J. Hoekstra, Highly-selective 4-(1,2,3-triazole)-based P450c17 α 17,20-lyase inhibitors, *Bioorg. Med. Chem. Lett.* 24 (2014) 2444–2447.
- S. Haider, P.B. Ehmer, S. Barassin, C. Batzl-Hartmann, R.W. Hartmann, Effects of novel 17 α -hydroxylase/C17,20-lyase (P45017, CYP17) inhibitors on androgen biosynthesis in vitro and in vivo, *J. Ster. Biochem. Mol. Biol.* 84 (2003) 555–562.
- M.K. Akhtar, S.L. Kelly, M.A. Kaderbhai, Cytochrome b5 modulation of 17 α hydroxylase and 17–20 lyase (CYP17) activities in stereogenesis, *J. Endocrinol.* 187 (2005) 267–274.
- L. Yin, Q. Hu, CYP17 inhibitors-abiraterone, C17,20-lyase inhibitors and multi-targeting agents, *Nat. Rev. Urol.* 11 (2014) 32–42.
- N.M. DeVore, E.E. Scott, Structures of cytochrome P450 17A1 with prostate cancer drugs abiraterone and TOK001, *Nature* 482 (2012) 116–120.
- I.M. Bird, D.H. Abbott, The hunt for a selective 17,20 lyase inhibitor; learning lessons from nature, *J. Steroid Biochem. Mol. Biol.* 163 (2016) 136–146.
- T.S. Vasaitis, R.D. Bruno, V.C.O. Njar, CYP17 inhibitors for prostate cancer therapy, *J. Steroid Biochem. Mol. Biol.* 125 (2011) 23–31.
- L. Gomez, J.R. Kovac, D.J. Lamb, CYP17A1 inhibitors in castration-resistant prostate cancer, *Steroids* 95 (2015) 80–87.
- J.S. De Bono, C.J. Logothetis, A. Molina, K. Fizazi, S. North, L. Chu, K.N. Chi, R.J. Jones, O.B. Goodman Jr, F. Saad, J.N. Staffurth, P. Mainwaring, S. Harland, T.W. Flaig, T.E. Hutson, T. Cheng, H. Patterson, J.D. Hainsworth, C.J. Ryan, C.N. Sternberg, S.L. Ellard, A. Flechon, M. Saleh, M. Scholtz, E. Efstathiou, A. Zivi, D. Bianchini, Y. Loriot, N. Chieffo, K. Thian, C.M. Haqq, H.I. Scher, Abiraterone and increased survival in metastatic prostate cancer, *N. Engl. J. Med.* 364 (2011) 1995–2005.
- T. Kaku, T. Hitaka, A. Ojida, N. Matsunaga, M. Adachi, T. Tanaka, T. Hara, M. Yamaoka, M. Kusaka, T. Okuda, S. Asahi, S. Furuya, A. Tasaka, Discovery of orteronel (TAK700), a naphthylmethylimidazole derivative, as a highly selective 17,20-lyase inhibitor with potential utility in the treatment of prostate cancer, *Bioorg. Med. Chem.* 19 (2011) 6383–6399.
- J.A.R. Salvador, R.M.A. Pinto, S.M. Silvestre, Steroidal 5 α -reductase and 17 α -hydroxylase/17,20-lyase (CYP17) inhibitors useful in the treatment of prostatic disease, *J. Steroid Biochem. Mol. Biol.* 137 (2013) 199–222.
- V.C. Njar, A.M. Brodie, Discovery and development of Galeterone (TOK-001 or VN/124-1) for the treatment of all stages of prostate cancer, *J. Med. Chem.* 58 (2015) 2077–2087.
- J.H. Alzate-Morales, A. Vergara-Jaque, J. Caballero, Computational study on the interaction of N1 substituted pyrazole derivatives with B-Raf Kinase: An unusual water wire hydrogen-bond network and novel interactions at the entrance of the active site, *J. Chem. Inf. Model.* 50 (2010) 1101–1112.
- P. Purushottamachar, A. Khandelwal, T.S. Vasaitis, R.D. Bruno, L.K. Gediya, V.C.O. Njar, Potent anti-prostate cancer agents derived from a novel androgen receptor down-regulating agent, *Bioorg. Med. Chem.* 16 (2008) 3519–3529.
- S. Bonomo, C.H. Hansen, E.M. Petrunak, E.E. Scott, B. Styrisshave, F.S. Jørgensen, L. Olsen, Promising tools in prostate cancer research: selective non-steroidal cytochrome P450 17A1 inhibitors, *Sci. Rep.* 6 (2016) 1–11.
- [Takeda announces termination of Orteronel (TAK-700) development for prostate cancer in Japan, USA and Europe, 2014 [Press release], <http://www.takeda.com/newsreleases> Accessed: 04/07/2018.
- I. Giangreco, D.A. Cosgrove, M.J. Packer, An extensive and diverse set of molecular overlays for the validation of pharmacophore programs, *J. Chem. Inf. Model.* 53 (2013) 852–866.
- C.G. Wermuth, C.R. Ganellin, P. Lindberg, L.A. Mitscher, ; “Glossary of terms used in medicinal chemistry (IUPAC Recommendations 1998)”, *Pure. Appl. Chem.* 70 (1998) 1129–1143.
- N.R. Tawari, M.S. Degani, Pharmacophore mapping and electronic feature analysis for a series of nitroaromatic compounds with antitubercular activity, *J. Comput. Chem.* 31 (2010) 739–751.
- D. Schuster, D. Kowalik, J. Kirchmair, C. Laggner, P. Markt, C. Aebischer-Gumy, F. Ströhle, G. Möller, G. Wolber, T. Wilckens, T. Langer, A. Odermatt, J. Adamski, Identification of chemically diverse, novel inhibitors of 17 β -hydroxysteroid dehydrogenase type 3 and 5 by pharmacophore-based virtual screening, *J. Steroid Biochem. Mol. Biol.* 125 (2011) 148–161.
- F. Xiao, M. Yang, Y. Xu, W. Vongsangnak, Comparisons of prostate cancer inhibitors abiraterone and TOK-001 binding with CYP17A1 through molecular dynamics, *Comput. Struct. Biotechnol. J.* 13 (2015) 520–527.
- E.M. Petrunak, N.M. DeVore, P.R. Porubsky, E.E. Scott, Structures of human steroidogenic cytochrome P450 17A1 with substrates, *J. Biol. Chem.* 47 (2014) 32952–32964.
- M.A.E. Pinto-Bazurco Mendieta, M. Negri, C. Jagusch, U. Müller-Vieira, T. Lauterbach, R.W. Hartmann, Synthesis, biological evaluation, and molecular modeling of abiraterone analogues: novel CYP17 inhibitors for the treatment of prostate cancer, *J. Med. Chem.* 51 (2008) 5009–5018.
- Y. Zhuang, B.G. Wachall, R.W. Hartmann, Novel imidazolyl and triazolyl substituted biphenyl compounds: synthesis and evaluation as nonsteroidal inhibitors of human 17 α -hydroxylase-C17, 20-lyase (P450C17), *Bioorg. Med. Chem.* 8 (2000) 1245–1252.
- Q. Hu, L. Yin, C. Jagusch, U.E. Hille, R.W. Hartmann, Isopropylidene substitution increases activity and selectivity of biphenylmethylene 4-pyridine type CYP17 inhibitors, *J. Med. Chem.* 53 (2010) 5049–5053.
- N.R. Budha, N. Mehrotra, R. Tangallapally, R.J. Qi, A.J. Daniels, R.E. Lee, B. Meibohm, Pharmacokinetically-guided lead optimization of nitrofuranylamine anti-tuberculosis agents, *Appl. J.* 10 (2008) 157–165.
- G.S. Deora, P. Joshi, V. Rathore, K.L. Kumar, R. Ohlyan, A. Kandale, Pharmacophore modelling and 3D QSAR analysis of isothiazolidinedione derivatives as PTP1B inhibitors, *Med. Chem. Res.* 22 (2013) 3478–3484.
- S.V. Jain, M. Ghate, K.S. Bhadoriya, S.B. Bari, G. Sugandhi, P. Mandwal, 3D-QSAR pharmacophore modelling and in silico screening of phospholipase A $_{2\alpha}$ inhibitors, *Med. Chem. Res.* 22 (2013) 3096–3108.
- S. Špirotić-Halilović, M. Salihović, E. Veljović, A. Osmanović, S. Trifunović, D. Završnik, Chemical reactivity and stability predictions of some coumarins by means of DFT calculations, *Bull. Chem. Technol. Bosn. Herz.* 43 (2014) 57–60.
- I. Fleming, *Frontier Orbitals and Organic Chemical Reactions*, John Wiley and Sons, New York, 1976.
- N.J. Gumedé, P. Singh, M.I. Sabela, K. Bisetty, L. Escuder-Gilabert, M.J. Medina-Hernández, S. Sagrado, Experimental-like affinity constants and enantioselectivity estimates from flexible docking, *J. Chem. Inf. Model.* 52 (2012) 2754–2759.
- G. Attard, A.S. Belledgrun, J.S. de Bono, Selective blockade of androgenic steroid synthesis by novel lyase inhibitors as a therapeutic strategy for treating metastatic prostate cancer, *BJU Int.* 96 (2005) 1241–1246.

- [51] M. Yamaoka, T. Hara, T. Hitaka, T. Kaku, T. Takeuchi, J. Takahashi, S. Asahi, H. Miki, A. Tasaka, M. Kusaka, Orteronel (TAK-700), a novel non-steroidal 17,20-lyase inhibitor: Effects on steroid synthesis in human and monkey adrenal cells and serum steroid levels in cynomolgus monkeys, *J. Steroid Biochem. Mol. Biol.* 129 (2012) 115–128.
- [52] D.B. Jacoby, M.D. Williams, A. Galeterone, Orteronel and Ketoconazole Exhibit Differential Inhibitory Effects on CYP17 and Steroidogenesis, Poster presentation, Tokai Pharmaceuticals, Inc. (2013).
- [53] L. Wang, Y. Deng, Y. Wu, B. Kim, D.N. LeBard, D. Wandschneider, M. Beachy, R.A. Friesner, R. Abel, Accurate modeling of scaffold hopping transformations in drug discovery, *J. Chem. Theory Comput.* 13 (2017) 42–54.
- [54] L. Wang, Y. Wu, Y. Deng, B. Kim, L. Pierce, G. Krilov, D. Lupyan, S. Robinson, M.K. Dahlgren, J. Greenwood, D.L. Romero, C. Masse, J.L. Knight, T.T. Steinbrecher, T. Beuming, W. Damm, E. Harder, W. Sherman, M. Brewer, R. Wester, M. Murcko, L. Frye, R. Farid, T. Lin, D.L. Mobley, W.L. Jorgensen, B.J. Berne, R.A. Friesner, R. Abel, Accurate and reliable prediction of relative ligand binding potency in prospective drug discovery by way of a modern free-energy calculation protocol and force field, *J. Am. Chem. Soc.* 137 (2015) 2695–2703.
- [55] H. Park, H. Jung, S. Mah, S. Hong, Systematic computational design and identification of low picomolar inhibitors of Aurora Kinase A, *J. Chem. Inf. Model.* 58 (2018) 700–709.
- [56] M.C. Ford, K. Babaoglu, Examining the Feasibility of Using Free Energy Perturbation (FEP+) in predicting protein stability, *J. Chem. Inf. Model.* 57 (2017) 1276–1285.
- [57] B. Kuhn, M. Tichý, L. Wang, S. Robinson, R.E. Martin, A. Kuglstatter, J. Benz, M. Giroud, T. Schirmeister, R. Abel, F. Diederich, J. Hert, Prospective evaluation of free energy calculations for the prioritization of Cathepsin L Inhibitors, *J. Med. Chem.* 60 (2017) 2485–2497.
- [58] Maestro, version 10.2, Schrödinger, LLC, New York, NY, 2015.
- [59] MacroModel, version 10.8, Schrödinger, LLC, New York, NY, 2015.
- [60] Phase, version 4.3, Schrödinger, LLC, New York, NY, 2015.
- [61] S.L. Dixon, A.M. Smondyrev, E.H. Knoll, S.N. Rao, D.E. Shaw, R.A. Friesner, PHASE: A new engine for pharmacophore perception, 3D QSAR model development, and 3D Database Screening. Methodology and Preliminary Results, *J. Comput. Aided Mol. Des.* 20 (2006) 647–671.
- [62] N.R. Tawari, M.S. Degani, Pharmacophore modelling and density functional theory analysis for a series of nitroimidazole compounds with antitubercular activity, *Chem. Biol. Drug Des.* 78 (2011) 408–417.
- [63] Virtual Screening Workflow. Schrödinger, LLC, New York, NY, 2015.
- [64] Jaguar, version 8.8, Schrödinger, LLC, New York, NY, 2015.
- [65] Induced Fit Docking Protocol, Schrödinger, LLC, New York, NY, 2015.
- [66] <http://www.enamine.net/> [accessed 05/11/2014].
- [67] S. Goutellea, M. Maurinc, F. Rougierb, X. Barbautb, L. Bourguignona, M. Ducherb, P. Mairea, The Hill equation: a review of its capabilities in pharmacological modelling, *Clin. Pharmacol.* 22 (2008) 633–648.
- [68] A.V. Hill, The possible effects of the aggregation of the molecules of haemoglobin on its dissociation curves, *J. Physiol.* 40 (1910) 4–7.